

Numerical Simulation of Shale Gas Production and Fracturing Fluid Distribution: Integration of  
Apparent Permeability and Secondary Fracture Network Modeling

by

Chuanyao Zhong

A thesis submitted in partial fulfillment of the requirements for the degree of

Master of Science

in

Petroleum Engineering

Department of Civil and Environmental Engineering  
University of Alberta

© Chuanyao Zhong, 2019

## Abstract

Complex flow mechanisms are encountered in shale matrix due to the presence of nanopores. Numerous apparent permeability models have been proposed to capture the ensuing non-Darcy flow behavior. However, these models are not readily available in most commercial reservoir simulators, and ignoring these mechanisms can potentially underestimate the overall matrix conductivity. During the hydraulic fracturing process, the fracturing fluid may cause water blockage, if the nearby secondary fractures subsequently close and get disconnected due to changes in effective stress distribution during flowback and production. The circumstances and detailed mechanisms associated with this phenomenon are still poorly understood. This work implements an explicit coupling strategy for integrating a pressure-dependent apparent permeability model and a dynamic secondary fracture closure process in the reservoir simulation. The numerical models are subsequently used to study the impacts of apparent permeability modeling, secondary fracture distributions and water blockage on gas production and water loss; the impacts of multiphase flow functions and shut-in durations on fluid retention are assessed.

A set of 3D reservoir models are constructed based on data obtained from the Horn River shale gas reservoir. A stochastic 3D discrete fracture network (DFN) model are upscaled into equivalent continuum dual-porosity dual-permeability (DPDK) models. An apparent permeability ( $K_{app}$ ) model accounting for the contributions of Knudsen diffusion, slip flow and surface pore roughness is applied at each grid block. In order to capture the pressure dependency, a novel coupling scheme is formulated to facilitate the updating of  $K_{app}$  and effective stress after a certain designated time interval. In addition, a novel method involving rock-type indicators is introduced to represent the open and closed states of secondary fractures, facilitating the modeling of stress-dependent closure of the secondary fracture system.

The results reveal that incorporating these additional flow mechanisms via the apparent permeability formulation could potentially increase the overall gas production prediction by up to 12%, depending on the matrix or fluid properties; ignoring  $K_{app}$  modeling could overestimate water recovery. Fracture closure and the resulting water blockage would reduce the gas production but enhance the water recovery. The implications of  $K_{app}$  and fracture closure modeling in water-loss mechanisms are further examined through a set of sensitivity analyses. A few interesting findings are observed: (1) the extent to which the fracturing fluid could imbibe into the matrix is mainly affected by the secondary fracture connectivity; an increase in secondary fracture intensity may enhance water loss; (2) except for an increase in the matrix gas relative permeability, gas and water productions are typically inversely related to the amount of water in the near-well region; (3) in a gas-water system, compressibility of the in-situ fluids renders the effects of countercurrent imbibition and water retention to be more complex from those observed in water-oil systems; (4) in the presence of disconnected secondary fractures, gas production would be improved with less water imbibition into the matrix, while a shorter shut-in period may be beneficial to both water and gas recovery. These results have offered several interesting insights regarding the potential implications on fracturing design and estimation of stimulated reservoir volume.

## **Preface**

This thesis is an original work by Chuanyao Zhong. Similar contents as Chapter 2 and Chapter 5 of this thesis can also be found in my conference paper which has been published as Zhong, C., & Leung, J., “Numerical Investigation of Water Blockage in Secondary Fractures and Apparent Permeability Modeling in Shale Gas Production,” paper URTEC-2019-592-MS presented at the Unconventional Resources Technology Conference, Denver, Colorado, USA, Jul. 22-24, doi:10.15530/urtec-2019-592.

*Dedicated to my parents (Xiaohong Zhong and Ying Wang) and all my family members for their love, endless support and encouragement.*

## **Acknowledgements**

First and foremost, I would like to send my sincere appreciation to Dr. Juliana Leung for her encouragement and support during my research. My work would not have been done without her wonderful guidance, inspiring enthusiasm, unlimited patience and insightful ideas during my entire research. I am also grateful to Dr. Doug Tomlinson, Dr. Hassan Dehghanpour and Dr. Wei (Victor) Liu for coming to my final defense as examining committee members and giving me constructive comments and suggestions.

I would like to thank all the professors in the department for teaching me the interesting knowledge and cutting-edge technologies regarding the petroleum engineering. In addition, I want to thank all the research members in Dr. Leung's group who encouraged, helped and inspired me through all the difficulties, and I would like to thank all the people who have ever helped me during my two-year MSc study.

My gratitude also goes to University of Alberta and Natural Sciences and Engineering Research Council of Canada (Discovery Grants Program: RGPIN-2017-05779) for providing the financial support. I would also like to thank the Computer Modeling Group Ltd. (CMG) and Golder Associates Ltd. for providing the academic licenses for IMEX and FracMan®, respectively.

Finally, I am truly grateful to my family, for their great love, endless support and encouragement.

# Table of Contents

Abstract.....	ii
Preface.....	iv
Acknowledgements.....	vi
Table of Contents.....	vii
List of Tables .....	ix
List of Figures .....	x
List of Symbols.....	xiii
Chapter 1: Introduction.....	1
1.1 Background .....	1
1.2 Problem Statement .....	3
1.3 Research Objectives .....	5
1.4 Thesis Outline .....	6
Chapter 2: Literature Review.....	8
2.1 Modeling of Apparent Permeability.....	8
2.2 Modeling of Secondary Fracture Network.....	10
2.3 Modeling of Secondary Fracture Closure .....	11
2.4 Sensitivity Analysis of Multiphase Flow Functions and Shut-in Durations .....	13
Chapter 3: Methodology .....	15
3.1 Base Model.....	15
3.1.1 Model Structure .....	15
3.1.2 Multi-Phase Flow Functions.....	16
3.1.3. Modeling of Hydraulic Fracturing Process .....	19
3.2 Integration of Secondary Fractures via Discrete-Fracture-Network (DFN) Models and Upscaling.....	20
3.3 Apparent Permeability Modeling.....	21
3.3.1 Fundamentals of Apparent Permeability Modeling.....	21
3.3.2 Dynamic Updating of Apparent Permeability .....	24
Chapter 4: Impacts of Secondary Fracture Network and $K_{app}$ Modeling.....	26
4.1. Example with Field Production Data .....	26

4.2. Impacts of Secondary Fracture Network.....	28
4.3. Impacts of Apparent Permeability Modeling.....	31
4.4. Sensitivity Analysis.....	33
4.4.1 Effects of Secondary Fracture Intensity .....	33
4.4.2 Effects of Reservoir Pressure and $K_{app}$ .....	34
4.4.3 Effects of Matrix Capillary Pressure ( $P_c$ ).....	36
4.4.4 Effects of Matrix Water Relative Permeability ( $K_{rw}$ ).....	38
4.4.5 Effects of Matrix Gas Relative Permeability ( $K_{rg}$ ).....	40
Chapter 5: Impacts of Secondary Fracture Closure .....	43
5.1 Modeling of Secondary Fracture Closure Using Rock-Type Indicators.....	43
5.2 Impacts of Secondary Fracture Closure on Fracturing Fluid Recovery.....	44
5.3 Sensitivity Analysis (Secondary Fracture Closure Considered) .....	51
5.3.1 Effects of Matrix Capillary Pressure .....	51
5.3.2 Effects of Matrix Water Relative Permeability .....	52
5.3.3 Effects of Matrix Gas Relative Permeability.....	53
5.3.4 Effects of Shut-in Duration.....	54
Chapter 6: Conclusions and Future Work.....	56
6.1 Conclusions .....	56
6.2 Future Work .....	58
Bibliography .....	61

## List of Tables

Table 1. Reservoir, well, and fluid properties for the base simulation model (Novlesky et al., 2011; Anderson et al., 2013; Nejadi et al., 2015). .....	16
Table 2. Probability distributions for DFN parameters. ....	20
Table 3. Parameters for the apparent permeability ( $K_{app}$ ) model.....	23
Table 4. Summary of the cases studied.....	28

## List of Figures

Figure 1. Illustration of the simulation domain – (a) 3D view; (b) top view.....	16
Figure 2. Multi-phase flow functions for the base model: (a), (b), and (c) relative permeability functions for hydraulic fracture, matrix and secondary fracture, respectively; (d) and (e) capillary pressure functions for matrix and secondary fracture.....	18
Figure 3. (a) DFN model and (b) equivalent dual-porosity dual-permeability model (the variable of fracture spacing (m) along the x-direction is shown). .....	20
Figure 4. $K_{app}$ as functions of (a) pressure and (b) average pore radius (examples). .....	24
Figure 5. Coupling of $K_{app}$ modeling and flow simulation. ....	24
Figure 6. Cumulative gas production for different updating frequencies (examples). .....	25
Figure 7. Comparison of production profiles between the field historical data and (a) Base Case and (b) Case A. ....	27
Figure 8. Profiles of (a) gas production and (b) water recovery for Case A and Case B. ....	29
Figure 9. Top view of the four regions selected for fluid-loss investigation [Region 1: inside HF; Region 2: matrix immediately adjacent to HF; Region 3: matrix in the near-well region (but not immediately adjacent to the HF); Region 4: matrix far away from HF]. .....	30
Figure 10. Effects of DFN modeling on average water saturation profiles: (a) Region 1, (b) Region 2, (c) Region 3, (d) Region 4.....	31
Figure 11. Profiles of (a) gas production and (b) water recovery for Case A and Case C. ....	32
Figure 12. Effects of $K_{app}$ modeling on average water saturation profiles: (a) Region 1, (b) Region 2, (c) Region 3, (d) Region 4.....	33
Figure 13. DFN models with different levels of fracture intensity: (a) water recovery, (b) average water saturation in region 4.....	34
Figure 14. (a) Cumulative gas production and (b) water recovery for the three pairs of cases with different initial reservoir pressure. ....	35

Figure 15. (a) Capillary pressure functions and (b) the corresponding cumulative gas production and water recovery profiles.....	36
Figure 16. Effects of matrix capillary pressure on water volumes in: (a) Region 1, (b) Region 2, (c) Region 3, (d) Region 4. ....	37
Figure 17. (a) Water relative permeability functions and (b) the corresponding cumulative gas production and water recovery.....	39
Figure 18. Effects of matrix water relative permeability on water volumes in: (a) Region 1, (b) Region 2, (c) Region 3, (d) Region 4.....	39
Figure 19. (a) Gas relative permeability functions and (b) the corresponding cumulative gas production and water recovery profiles. ....	41
Figure 20. Effects of matrix gas relative permeability on average water saturation profiles: (a) Region 1, (b) Region 2, (c) Region 3, (d) Region 4.....	41
Figure 21. Coupling of secondary fracture closure modeling and flow simulation.....	44
Figure 22. Comparison of production profiles between the field historical data and Case D. ....	45
Figure 23. Comparison between Case D and Case E in terms of (a) gas production and (b) water recovery.....	46
Figure 24. Top view of water saturation maps of (a) the near-well secondary fracture system and (b) matrix system at different dates in Case D.....	47
Figure 25. Top view of closed fracture cells in the near-well region at different production dates in Case D.....	48
Figure 26. (a) Change in gas volume with time in the near-well secondary fracture; (b) gas production profiles of Case D and Case E; (c) change in water volume with time in the near-well matrix; (d) water production profiles of Case D and Case E; and (e) change in average matrix pressure in the near-well region.....	50
Figure 27. (a) Cumulative gas production; (b) gas volume in near-well secondary fractures; and (c) water volume in the near-well matrix corresponding to various matrix capillary pressure functions.....	52

Figure 28. (a) Cumulative water recovery and (b) water volume in the near-well matrix corresponding to various matrix water relative permeability functions. .... 53

Figure 29. (a) Cumulative gas production and (b) gas volume in near-well matrix corresponding to different matrix gas relative permeability functions. .... 54

Figure 30. (a) Cumulative gas production; (b) gas volume in near-well secondary fractures; and (c) water volume in the near-well matrix corresponding to various shut-in durations (12, 8 and 2 weeks). .... 55

## List of Symbols

$a_{HF}$  = Initial hydraulic fracture aperture, m

$a_1$  = Empirical constant representative for low-permeability reservoirs

$a_2$  = Empirical constant representative for low-permeability reservoirs

$a_3$  = A measure of pore structure

$B$  = Boltzmann constant, J/K

$c_t$  = Rock compressibility, Pa<sup>-1</sup>

$D_f$  = Fractal dimension of the pore surface

$D_k$  = Knudsen diffusion coefficient

$k_M$  = Matrix permeability, m<sup>2</sup>

$k_{HF}$  = Hydraulic fracture permeability, m<sup>2</sup>

$k$  = Permeability, md

$k_D$  = Darcy permeability, m<sup>2</sup>

$K_{app}$  = Apparent permeability in porous media, m<sup>2</sup>

$K_n$  = Knudsen number

$M$  = Molar mass of methane, kg/kmol

$P_i$  = Initial reservoir pressure, Pa

$P_{fi}$  = Initial fracture pressure, Pa

$P_{wf}$  = Minimum wellbore flowing pressure, Pa

$P_c$  = Capillary pressure, Pa

$P$  = Reservoir pressure, Pa

$P_{critical\ methane}$  = Critical pressure of methane, Pa

$R$  = Universal gas constant, J/mol/K

$R_{avg}$  = Average pore radius, m

$R_{methane}$  = Molecule diameter of methane, m

$R_{methane\ collision}$  = Collision diameter of methane, m

$S_{wM}$  = Matrix initial water saturation

$S_{wHF}$  = Hydraulic fracture initial water saturation

$S_w$  = Water saturation

$T$  = Temperature, K

$T_{critical\ methane}$  = Critical temperature of methane, K

### *Greek Symbols*

$\alpha$  = Tangential momentum accommodation coefficient

$\mu$  = Gas viscosity, Pa·s

$\rho_{avg}$  = Gas density, kg/m<sup>3</sup>

$\sigma'$  = Interfacial tension between water and gas, dynes/m

$\phi_M$  = Matrix porosity

$\phi_{HF}$  = Hydraulic fracture porosity

$\phi$  = Porosity

$\tau$  = Tortuosity

$\delta'$  = Ratio of normalized molecular size to local average pore diameter

# Chapter 1: Introduction

This chapter presents the background of the shale gas resources and its extraction technique, problem statement, research objective and thesis outline.

## 1.1 Background

Shale gas is a natural gas found in the shale rock, it has become one of the most important sources of energy supply in the North America in recent years (Khlaifat et al., 2011). Take the United States as an example, the “revolution of shale gas” was a phenomenon at the beginning of this century, which has significantly influenced the gas market of the world and improved the country’s economy (Le, 2018). However, for Canada, the commercial production of shale gas is still at the very early stage; it is estimated that between 550 and 860 trillion cubic feet of gas could potentially exist in the shale gas formations in Western Canada (Javadpour et al., 2007).

Shale gas reservoirs are continuous, non-buoyancy driven hydrocarbon plays that are composed of different fine-grained sedimentary rocks (e.g., true shales, mudrocks, limestones, siltstones) (Chalmers et al., 2012; Gensterblum et al., 2015). In the shale gas reservoirs, the size of the pores is usually at the nanoscale. Shale gas is stored in three main forms in the nanopores at in-situ conditions: free gas, adsorbed gas and dissolved gas (Zhang et al., 2018). Unlike conventional oil and gas reservoirs, shale gas reservoirs are characterized by extremely low permeability (typically 10 to 100 nanodarcies) and porosity, although various gas flow mechanisms, including Knudsen diffusion and slip flow, may contribute significantly to the overall gas conductivity.

Due to the reservoir’s ultralow matrix conductivity, one of the most common extraction techniques

for shale gas development is hydraulic fracturing, during which a horizontal well is drilled, a large amount of fracturing fluid is injected and a shut-in/soaking period is followed, such that both in-situ gas and fracturing fluid are redistributed in the system (Ning et al., 1993; Mayerhofer and Meehan, 1998; Reinicke et al., 2010; McClure and Zoback, 2013; McClure, 2014). However, only a portion of the fracturing fluid (typically < 50%) could be recovered during the flow-back process after the well is re-opened (McClure, 2014; Cheng, 2012; Wattenbarger and Alkough, 2013; Makhanov et al., 2014).

Shale formation often exhibits a high degree of natural fracturing. In the case of the Horn River gas reservoirs, the shale package is, on average, comprised of 60% quartz, rendering the rock to be very brittle (Novlesky et al., 2011). Pre-existing natural fractures could be reactivated through extension, dilation and shearing during the hydraulic fracturing process, as they are often optimally oriented, relative to the in-situ stress field (Rogers et al., 2010). They also influence the behavior related to hydraulic fracture initiation and propagation; the resultant complex network involving both hydraulic and secondary fractures often plays an important role in providing an adequate connection between the wellbore and the formation to transmit reservoir fluids (Meyer and Bazan, 2011; Yu and Sepehrnoori, 2014b). The role of natural and secondary fractures as fluid-flow pathways are known to be significant (Hunter and Young, 1953; Wilkinson, 1953; Barfield et al., 1959).

However, the induced fractures could be closed when the fluid pressure inside the fracture drops below the minimum horizontal stress (fracture closure pressure). Fracture closure pressure refers to the minimum pressure required to keep the fracture open, which also represents the pressure at which the fracture would close in the absence of any proppant; in many cases, the closure pressure could be assumed to be the same as the minimum horizontal stress (Belyadi et al., 2019). In the

shale gas reservoirs, due to the change in effective stress distribution, the nearby secondary fractures could be closed and get disconnected with the main fracture during flowback and production; the fluid inside the fractures could also get squeezed out upon fracture closure; as the fracture network is disconnected, gas is being produced from the matrix, the water accumulated in the near-well region could hinder the gas flow due to the reduction in gas relative permeability for a high water saturation (water blockage) (Sherman and Holditch, 1991; Shanley et al., 2004; Shaoul et al., 2011; Ehig-Economides et al., 2012; McClure and Horne, 2014).

Therefore, the hypothesis of my research is that the matrix apparent permeability and secondary fracture closure should have a significant impact on both hydrocarbon production and fracturing fluid flow-back performance. To test the hypothesis, I would create a way of incorporating the matrix apparent permeability modeling and stress-dependent secondary fracture closure in the shale gas reservoir simulation; and I would demonstrate their impacts on both gas and fracturing fluid recovery; then the sensitivity analysis on matrix multiphase flow functions and operational strategies would be done by using my new models.

## **1.2 Problem Statement**

The efficiency of fracturing fluid recovery and gas production is highly affected by fracture properties (e.g., secondary fracture distributions, fracture closure) and matrix properties (e.g., matrix conductivity, capillary pressure, multiphase flow functions). Currently, the modeling of the shale gas reservoirs is encountering some challenges.

The first challenge is the coupling of the complex non-Darcy flow physics and randomly distributed fracture network in the shale gas reservoir modeling. The interplay between these non-

Darcy phenomena and secondary (natural) fracture distribution on gas production and water loss could play an important role on optimizing operational strategies in the hydraulic-fracturing operation. However, these two factors are often ignored in many reservoir simulation studies, which may result in the under-/over-estimation of overall gas production and fracturing fluid loss (McClure, 2014; Makhanov et al., 2014; Wang and Leung, 2015a, b; Liu et al., 2017).

The second challenge is the modeling of the fracture closure behavior and its dynamic closure process due to the change in in-situ stress. It was indicated that closure and reactivation of near-well secondary fractures may have significant impacts on gas flow and fracturing fluid recovery, but the circumstances and detailed mechanisms associated with this phenomenon are still poorly understood.

The third challenge is integrating and analyzing the mentioned effects (e.g., fracture distributions, fracture closure and non-Darcy flow physics) all together in the shale gas reservoir modeling. These are the reasons why the analytical models (e.g., Rate Transient Analysis method) could be limited. Therefore, how to couple all the mentioned effects in a numerical study should be investigated.

In addition, the sensitivity analysis of the multiphase flow functions is still less understood for shale gas reservoirs: imbibition plays an important role in fracturing fluid recovery because of the high capillary pressure in shale gas reservoirs, but whether imbibition will be beneficial or detrimental to subsequent gas and water production should be further investigated; besides, it is anticipated that the relative permeability could also significantly influence the fluids distributions, the detailed studies of how water and gas relative permeability affect the gas and water production are still lacking.

Last, the hydraulic fracturing flow back operation should be optimized as shut-in duration could significantly impact the production performance.

### **1.3 Research Objectives**

The objective of this research is to investigate different water loss mechanisms, their influence on subsequent gas production and provide fracturing flow back operational strategy by using numerical simulation method which incorporates the effects of secondary fracture networks, fracture closure and non-Darcy flow mechanisms, which entails:

- (1) Create a novel, yet practical, coupling scheme to facilitate the updating of pressure-dependent matrix apparent permeability in numerical simulation of shale gas production, to capture the non-Darcy flow behavior due to the transport mechanisms taken place in the nanopores.
- (2) Incorporate the realistic configurations of stochastic 3D discrete network models (DFN) in the reservoir simulation.
- (3) Create a novel method to facilitate the modeling of the stress-dependent closure of the secondary fracture system in our reservoir simulation.
- (4) Calibrate our numerical model by using the field data corresponding to a well drilled in the Horn River basin.
- (5) Examine the fracturing fluid loss behavior by simulating the hydraulically fractured shale gas reservoir which considers the impacts of secondary fracture distributions and multiple gas flow mechanisms, and to explore potential implications on the prediction of stimulated reservoir volume and fracturing design.

(6) Analyze the sensitivities of reservoir pressure, fracture intensity, matrix multiphase flow functions (capillary pressure and water/gas relative permeability) and shut-in durations.

(7) Assess whether secondary fracture closure would contribute to water blockage or enhance imbibition, with potential implications on the prediction of reservoir volume and optimization of operational strategies.

## **1.4 Thesis Outline**

This thesis consists of six chapters. The outline of these chapters is provided as follows:

Chapter 1 presents the background of shale gas resources and its extraction technique; problem statement and research objectives are also presented in this chapter.

Chapter 2 presents the literature review including the existing studies on apparent permeability modeling, secondary fracture network modeling, fracture closure modeling, sensitivity analysis of multiphase flow functions and shut-in durations, and their drawbacks.

Chapter 3 presents the methodology used in this study including mechanistic numerical model construction, secondary fracture network integration and apparent permeability modeling.

Chapter 4 presents the validations of our numerical model by using the field data of a well; and the investigations on the impacts of secondary fracture network and apparent permeability modeling on gas production and fracturing fluid recovery; sensitivity analysis is also presented.

Chapter 5 presents the methodology used for coupling the dynamic closure process of secondary fractures; the impacts of secondary fracture closure on gas production and fracturing fluid recovery are discussed; sensitivity analysis is also presented.

Chapter 6 presents the conclusions and recommendations for future work.

## Chapter 2: Literature Review

In this chapter, the literatures regarding the existing studies on apparent permeability modeling, secondary fracture network modeling, fracture closure modeling, sensitivity analysis of multiphase flow functions and shut-in durations, and their drawbacks are reviewed.

### 2.1 Modeling of Apparent Permeability

As mentioned in the previous section, in nano-sized pores, various gas flow mechanisms may contribute significantly to the overall gas conductivity. The dimensionless Knudsen number ( $K_n$ ), which is defined as the ratio of gas mean-free-path and the macroscopic length scale of a physical system, is widely used for identifying the corresponding flow regimes (Zhong et al., 2015; Roy et al., 2003).  $K_n < 10^{-3}$  corresponds to continuum flow that is described by conventional Darcy's law: the movement of gas is driven via filtration without significant impacts due to gas molecules' interactions with the pore surfaces or that of the adsorption layer; for  $10^{-3} < K_n < 10^{-1}$ , the flow regime is identified as slip flow, where collisions with other gas molecules and the pore surfaces are substantial, such that the speed at which the gas molecules are moving inside the pore space is comparable to that on the pore walls; for  $10^{-1} < K_n < 10$ , the flow regime is classified as transitional flow regime, where both slip flow and Knudsen diffusion must be considered; finally, for  $K_n > 10$ , the flow regime is referred to as Knudsen diffusion, where gas molecules are moving through the pore network via diffusion, and this diffusive flow behavior is discovered by Knudsen in 1909 (Knudsen, 1909).

The pressure dependency of these gas transport mechanisms have been widely reported and analyzed (Wang and Li, 2004). Dong et al. (2010) observed in their experimental study that

apparent permeability of the shale was reduced from  $2 \times 10^{-17}$  to  $1 \times 10^{-19}$  m<sup>2</sup> when the confining pressure increased from 3 to 120 MPa, at a constant pore pressure at 0.1 MPa. Mckernan et al. (2014) also demonstrated that the gas apparent permeability would reduce by two orders of magnitude, as the effective stress increased from 7 to 10 MPa.

The assumption of Darcy flow is invalid when attempting to capture these nano-scale flow physics (Civan et al., 2011). Instead, many apparent permeability models have been proposed, which take into account these non-Darcy flow physics and their stress dependency. Javadpour (2009) developed an apparent permeability model incorporating Knudsen diffusion and slip flow for a set of straight cylindrical nanotubes. Darabi et al. (2012) later presented an improvement, where a single nanotube system was upscaled to an ultra-tight porous medium, such that gas flow through an interconnected network of micropores and nanopores was studied, and effects of surface roughness were considered. Other models were also developed to capture additional gas transport mechanisms: for instance, Civan (2010) introduced a model that accounts for continuum, slippage, transition and free-molecular flows; Sakhaee-Pour and Bryant (2012) developed a model that incorporates the contributions of slippage and adsorbed layers. Other studies focused on the modeling of real gas flow: Azom and Javadpour (2012) modified the original model from Javadpour (2009) for real gas flow; Shi et al. (2013) proposed a model where effects of water film adhering to the inorganic pores were incorporated; Wu et al. proposed a model to describe surface diffusion of adsorbed gas (2015a) and another model for real gas transport through nanopores of varying cross-section shapes (2015b); Song et al. (2017) developed a model incorporating multiple transport mechanisms for real gas flow in nano-scale organic pores. Unfortunately, these models are not adopted in most commercial reservoir simulators.

Recently, Rubin et al. (2019) incorporated a dynamic matrix permeability updating step in their reservoir simulation study using an empirical apparent permeability model; their results certainly demonstrated that gas production and proppant requirement could be overestimated if gas slippage and matrix compaction were ignored; however, the presence of secondary fractures were not addressed in that study.

## **2.2 Modeling of Secondary Fracture Network**

A discrete-fracture-network (DFN) model can be constructed by use of statistical description of various input parameters, including fracture intensity, length, azimuth, aperture and transmissivity (Dershowitz et al., 2010). To model fluid flow in fractured porous media, one approach is to represent and discretize the fracture and matrix systems explicitly in the computational domain, where the fracture cells are assigned higher porosity and permeability values (Karimi-Fard et al., 2004; Aziz and Settari, 1979; Qasem et al., 2008; Rubin, 2010). The alternative approach is the dual-porosity method, in which an equivalent continuum medium is used. The concept was first introduced by Barenblatt and Zelthov (1960), and was further described by Warren and Root (1963). Many physical mechanisms, including water imbibition, molecular diffusion, and convection along the fractures, have been incorporated over the years (Sabathier et al., 1998). Others have adopted a hybrid approach: flow within the dominant connected fracture network is represented explicitly, while the smaller secondary fractures are represented via the dual-porosity framework (Nejadi et al., 2015; Wang and Leung, 2015a, b). A static and analytical upscaling, such as the one in Oda (1985), can be used to attain an equivalent dual-porosity; the main disadvantage of this static upscaling scheme is that it is limited to densely populated and well-connected fractures, as neither fracture connectivity nor size could be considered (Dershowitz et

al., 2000). This assumption is justifiable for shale reservoir, where the natural fracture intensity is often quite high (Nejadi et al., 2015).

### **2.3 Modeling of Secondary Fracture Closure**

Previous experimental studies have illustrated that fracture conductivity (i.e., aperture and permeability) would reduce with increasing effective stress (Huo et al., 2014). Several models were proposed to quantify the loss of conductivity due to fracture closure: Gangi (1978) proposed a “bed of nail” model where fracture closure is represented by deformation of surface asperities, while Walsh (1965) presented a model where fracture closure due to elastic deformation of the surrounding matrix and the ensuing changes in effective stress is described; another model developed by Schrauf and Evans (1986) described a closure mechanism due to the shear contact behavior of fracture surfaces. The presence of surface asperities is likely to have a significant effect on the fracture closure process in natural fractures, resulting in smaller, partially-closed, sub-fractures (Batzle, 1980); this issue regarding surface asperities, however, may not be overly relevant for secondary fractures that are created artificially, as they tend to have more even surfaces (Batzle, 1980). This study focuses primarily on the impact of fracture closure in the near-well region, where secondary fractures are mainly induced by the hydraulic fracturing process; therefore, partial closure due to surface asperities is not considered.

Numerical simulation is often a useful tool to examine the geomechanics effects (e.g., fracture closure) and their impacts on water loss. McClure (2014) coupled geomechanical and flow simulations to study water loss during flowback; they indicated that the fracture closure and the trapping of fluid away from the main hydraulic fracture could reduce water recovery; however, the

model was based on single-phase flow and various important factors, such as fracture intensity and matrix multi-phase flow functions, were not examined. In the simulation study by Wang and Leung (2015a, b), an empirical correlation of fracture conductivity as a function of fluid pressure (assuming constant overburden stress) was employed; the model used in their study was limited to 2D, but the results suggested that secondary fractures that were not directly connected to the hydraulic fracture would still provide conductive flow paths for fracturing fluid in the system; their results also suggested that secondary fractures that are water-filled initially can enhance counter-current imbibition. However, the dynamic closure of open fractures during the soaking and production periods was not addressed.

Additional modeling studies have examined the mechanisms associated with fracture closure and fluid loss. Sherman and Holditch (1991) described that rapid fracture closure due to pressure drawdown would result in fracturing fluid trapping and gas production reduction. It is illustrated by Ehig-Economides et al. (2012) that water-filled microfractures could potentially lose contact with the main hydraulic fracture due to closure of the induced secondary fractures during flowback. Similar conclusions were obtained by McClure and Horne (2014), who observed that fluid could be trapped in secondary fractures that are located far away from the wellbore. Increased fluid retention (i.e., water saturation), which is also referred to as water blockage, could contribute to a reduction in gas relative permeability and hinders gas flow to the well (Shaoul et al., 2011). Shanley et al. (2004) demonstrated that gas production would reduce dramatically if the water saturation exceeds 40-50% near the fracture faces.

## 2.4 Sensitivity Analysis of Multiphase Flow Functions and Shut-in Durations

Sensitivity analyses of matrix multiphase flow functions (e.g., capillarity and relative permeability) and shut-in durations pertinent to fluid loss mechanisms in unconventional reservoirs were conducted. As more water accumulated in the near-well region due to the counter-current imbibition, the gas flow could be hindered due to the reduction in gas relative permeability for a high water saturation (water blockage); however, the imbibition could also result in more gas being displaced to the secondary fractures and getting produced quickly after the well is opened (Ghanbari and Dehghanpour, 2016); Cheng (2012) presented a single-porosity model consisting of eight stages of hydraulic fracturing, but capillary pressure in the fracture cells was ignored. Wattenbarger and Alkough (2013) constructed a similar single-porosity model, where secondary fractures and matrix were assigned with identical relative permeability and capillary pressure functions. Fakcharoenphol et al. (2013) employed a hybrid model, where an equivalent secondary fracture and matrix dual-porosity model was used to represent a system of non-organic or organic matrix with interconnected network. The following conclusions can be derived from these studies: (1) an increase in fracture intensity and fracture width would lead to larger water retention in the secondary fractures; (2) imbibition is reduced when water relative permeability in secondary fractures or matrix is reduced; (3) initial gas rate is increased as a result of extended shut-in. A particular drawback of these studies is that the secondary fracture network was fully-connected and symmetrical. Wang and Leung (2015a, b) generated a hybrid model from multiple realizations of stochastic discrete fracture networks; different capillary pressure and relative permeability functions were assigned to the hydraulic fracture, secondary fracture and matrix cells, respectively. Similar to the previous studies, it was also observed that imbibition was reduced when matrix water relative permeability or capillary pressure was decreased; a prolonged shut-in duration may

enhance the short-term oil production but improvement for long-term production was not observed. However, a key observation was noted: although improved imbibition could enhance early production rate, while hindering water recovery, long-term production was not affected. They also found that cumulative oil production is highly influenced by the oil relative permeability. Unfortunately, the model used in their study was limited to 2D oil reservoir and only orthogonal fractures on a Cartesian mesh were considered.

## Chapter 3: Methodology

In this chapter, the methodology used for constructing the mechanistic model, integrating the secondary fracture network, incorporating the apparent permeability modeling in our numerical simulation is introduced.

### 3.1 Base Model

#### 3.1.1 Model Structure

A 3D (100 m × 1024 m × 120 m) hydraulically-fractured shale-gas production model is constructed in an adaptive implicit-explicit black-oil simulator, as illustrated in Figure 1 (CMG, 2016). Table 1 summarizes the reservoir, fluid and well properties, which are obtained from several field data sets corresponding to the Horn River shale formation (Novlesky et al., 2011; Anderson et al., 2013; Nejadi et al., 2015). All hydraulic fracture stages are assumed to be evenly spaced and symmetrical in this study, and only one hydraulic fracturing stage is simulated here. The entire domain is discretized into  $51 \times 55 \times 10$  grid blocks along the x-, y-, and z-directions, respectively. Local grid refinement is applied in the near-well regions. The production well is situated at the intersection of the hydraulic fracture and the horizontal well.

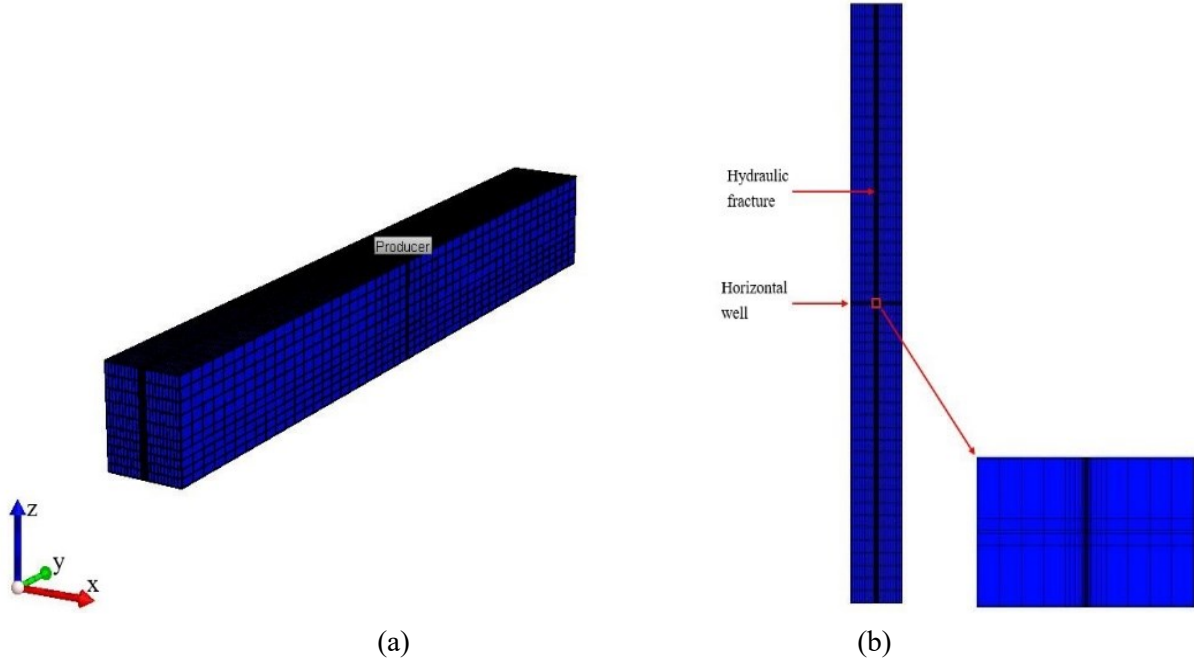


Figure 1. Illustration of the simulation domain – (a) 3D view; (b) top view.

**Table 1**

Reservoir, well, and fluid properties for the base simulation model (Novlesky et al., 2011; Anderson et al., 2013; Nejadi et al., 2015).

Parameters	Values
Initial reservoir pressure, $P_i$	$3.40 \times 10^7$ Pa
Initial fracture pressure, $P_{fi}$	$5.50 \times 10^7$ Pa
Minimum wellbore flowing pressure, $P_{wf}$	$1.00 \times 10^7$ Pa
Rock compressibility, $c_t$	$2.50 \times 10^{-9}$ Pa <sup>-1</sup>
Initial matrix permeability, $k_M$	$5.00 \times 10^{-20}$ m <sup>2</sup>
Matrix porosity, $\phi_M$	0.045
Initial matrix water saturation, $S_{wM}$	0.25
Hydraulic fracture permeability, $k_{HF}$	$9.87 \times 10^{-11}$ m <sup>2</sup>
Hydraulic fracture porosity, $\phi_{HF}$	1
Initial hydraulic fracture water saturation, $S_{wHF}$	1
Initial hydraulic fracture aperture, $a_{HF}$	0.03 m

### 3.1.2 Multi-Phase Flow Functions

Different relative permeability functions for two-phase gas-water flow are assigned to the matrix and hydraulic fracture systems according to Liu et al. (2017), as presented in Figure 2 (a) and (b).

Negligible capillary pressure ( $P_c$ ) is assigned in hydraulic fracture because of its high conductivity,

while capillary pressure function for the matrix is assigned according to Eq. (1), which is an empirical relationship proposed by Gdanski et al. (2009) based on the “Leverett J-function” (Leverett, 1941).

$$P_c = \frac{\sigma'}{a_2 (S_w)^{a_1}} \left( \frac{\phi}{k} \right)^{a_3} \times 6894.76 \dots\dots\dots(1)$$

where  $P_c$  [Pa] is the capillary pressure; the interfacial tension between water and gas ( $\sigma'$ ) is 40 dynes/m; the empirical constants of  $a_1 = 1.86$  and  $a_2 = 6.42$  are representative for low-permeability reservoirs (Gdanski et al., 2009; Holditch 1979); value of 0.5 is assigned for  $a_3$ , which is a measure of pore structure (Bradley, 1987);  $S_w$  is the water saturation;  $\phi$  is the matrix porosity;  $k$  [md] is permeability.

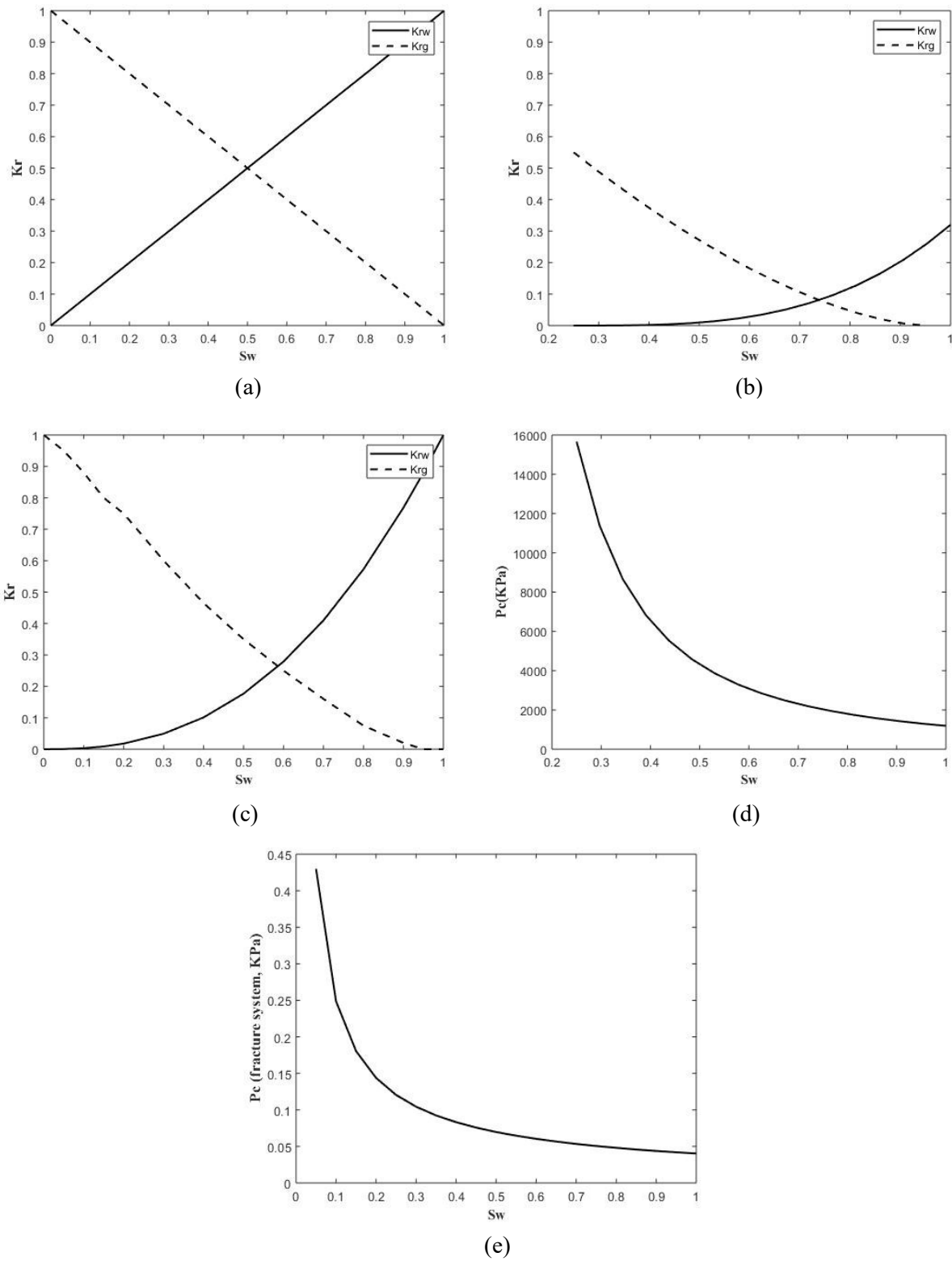


Figure 2. Multi-phase flow functions for the base model: (a), (b), and (c) relative permeability functions for hydraulic fracture, matrix and secondary fracture, respectively; (d) and (e) capillary pressure functions for matrix and secondary fracture.

### 3.1.3. Modeling of Hydraulic Fracturing Process

The numerical model developed here is intended to simulate the soaking, flow-back, and production periods immediately following hydraulic fracturing. To simulate the process of hydraulic fracturing, many previous simulation studies would incorporate an initial injection period into a pre-existing hydraulic fracture with an initial porosity of less than unity; however, some fluid leak-off may have already occurred during the injection stage (prior to the soaking period) and the use of a pre-existing hydraulic fracture implies that a post-closure state with no explicit consideration of change in effective stress must be assumed (Agrawal and Sharma, 2015; Gdanski et al., 2009; Alkough et al., 2014; Ghanbari and Dehghanpour, 2016; Wang and Leung, 2015a, b). In this study, an alternative method is adopted: instead of simulating the injection period, the in-situ condition immediately following hydraulic fracture is modeled by assigning the initial pressure inside the hydraulic fracture to be the same as the minimum horizontal stress; the hydraulic fracture is assumed to be evenly propped, completely open with an initial porosity of unity, and filled with water (Liu et al., 2017; 2019). Fracture closure of the main hydraulic fracture during the soaking and flowback periods would cause the fracturing fluid that was initially inside the hydraulic fracture to re-distribute into the nearby regions. It should be noted that fluid leak-off during the fracture-propagation stage is ignored in this approach. This simplification is justifiable, as this volume is typically very small, given that the propagation phase is quite short (approximately a few hours), and the corresponding leak-off coefficient is extremely low in shale reservoirs (on the order of  $1 \times 10^{-5}$  ft/min) (Shiozawa and McClure, 2016; Wu and Olson, 2016).

## 3.2 Integration of Secondary Fractures via Discrete-Fracture-Network (DFN)

### Models and Upscaling

As shown in Figure 3 (a), a realization of 3D discrete fracture network (DFN) model is constructed based on the probability distributions of various secondary fracture properties (i.e., intensity, length, height, aperture and permeability). These probability distributions, as summarized in Table 2, are inferred from several previous studies of the Horn River shale gas formations (Gale et al., 2014; Nejadi et al., 2015; Yang et al., 2018).

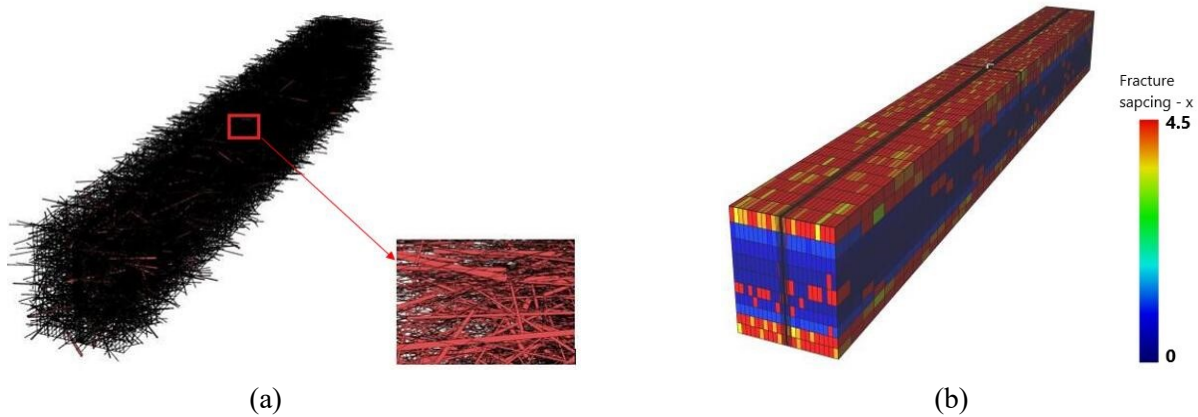


Figure 3. (a) DFN model and (b) equivalent dual-porosity dual-permeability model (the variable of fracture spacing (m) along the x-direction is shown).

**Table 2**

Probability distributions for DFN parameters.

Parameters	Probability distributions	Data Sources
Fracture intensity	Normal distribution, mean: 0.0226 1/m, std dev: 0.0043 1/ft	Nejadi et al., 2015
Fisher concentration distribution	Constant distribution, 10, dimensionless	Nejadi et al., 2015
Fracture length	Normal distribution, mean: 49.5800 m, std dev: 15.8300 m	Nejadi et al., 2015
Fracture height	Normal distribution, mean: 0.9144 m, std dev: 0.9053 m	Gale et al., 2014
Fracture aperture	Normal distribution, mean: 0.0003 m,	Yang et al., 2018

	std dev: 0.0002 m	
Fracture permeability	Normal distribution, mean: $2.4673 \times 10^{-14} \text{ m}^2$ , std dev: $2.4673 \times 10^{-14} \text{ m}^2$	Nejadi et al., 2015
Fracture compressibility	Constant distribution, $3.3511 \times 10^{-4} \text{ 1/Pa}$	Nejadi et al., 2015
Fracture porosity	Constant distribution, $1 \times 10^{-4}$ , dimensionless	Nejadi et al., 2015

The 3D DFN model is upscaled into an equivalent continuum dual-porosity dual-permeability model following Oda analytical approach (Oda, 1985), as shown in Figure 3 (b). Equivalent sigma factors and fracture permeability tensors obtained from Oda upscaling are provided as inputs in the DPDK reservoir simulation model. Other relevant properties for the secondary fracture system, such as rock compaction properties and relative permeability functions (Figure 2d) are obtained from Nejadi et al. (2015) and Farah (2016), respectively. Capillary pressure in the secondary fracture system is shown in Figure 2 (e), which is also computed in accordance to Eq. (1), where  $a_1 = 0.79$ ,  $a_2 = 321.67$  and  $a_3 = 0.5$  are used (Wang and Leung, 2015a, b). It is further assumed in our simulation that the initial water saturation in the secondary fracture is the same as the irreducible water saturation.

### 3.3 Apparent Permeability Modeling

#### 3.3.1 Fundamentals of Apparent Permeability Modeling

An apparent permeability ( $K_{app}$ ) [ $\text{m}^2$ ] function (Eqs. 2-4) proposed by Darabi et al. (2012), which is modified from the original model of Javadpour (2009), is adopted here. The model has incorporated contributions of Knudsen diffusion and slip flow, as well as accounting for the effects of surface pore roughness, and it is used to calculate the pressure-dependent apparent permeability in the matrix.

$$K_{app} = \frac{\mu M}{RT \rho_{avg}} \frac{\phi}{\tau} (\delta')^{D_f-2} D_k + k_D \left(1 + \frac{b}{P}\right) \dots\dots\dots (2)$$

where,

$$D_k = \frac{2R_{avg}}{3} \left(\frac{8RT}{\pi M}\right)^{0.5} \dots\dots\dots (3)$$

$$b = \left(\frac{8\pi RT}{M}\right)^{0.5} \frac{\mu}{R_{avg}} \left(\frac{2}{\alpha} - 1\right) \dots\dots\dots (4)$$

$$\alpha = \log_{10}(1 + K_n^{0.7}) \dots\dots\dots (5)$$

$$K_n = \frac{BT}{\sqrt{2\pi} R_{avg} (R_{methane\ collision})^2 P} \dots\dots\dots (6)$$

$$\delta' = \frac{R_{methane}}{2R_{avg}} \dots\dots\dots (7)$$

The first term in Eq. 2 represents the Knudsen diffusion at temperature  $T$  [K] and pressure  $P$  [Pa] for a gas with density of  $\rho_{avg}$  [kg/m<sup>3</sup>], and it incorporates the ratio of porosity to tortuosity ( $\phi/\tau$ ) that controls Knudsen flow in porous media (Javadpour et al., 2007); the second term corresponds to the slip flow.  $\delta'$  refers to the ratio of normalized molecular size to local average pore diameter. The impact of surface roughness is captured by  $D_f$ , which is the fractal dimension of the pore surface: it takes a value between 2 (smooth surface) and 3 (space-filling surface) (Coppens, 1999; Coppens and Dammers, 2006).  $D_k$  is the Knudsen diffusion coefficient in porous media, and it is a function of the average pore radius,  $R_{avg}$  [m], which can be inferred from experimental measurements.  $k_D$  [m<sup>2</sup>] =  $R_{avg}^2/8$  is the absolute Darcy permeability.  $\alpha$ , which is a function of the Knudsen number or  $K_n$ , denotes the tangential momentum accommodation coefficient (TMAC), which is dependent on temperature, pressure, gas compositions and wall surface smoothness: its value varies between 0 and 1, representing specular accommodation and diffuse accommodation, respectively (Arkilic et al., 2001). Parameters for the  $K_{app}$  modeling are summarized in Table 3, and they are inferred from previous studies of the Horn River shale gas reservoirs (Prausnitz and Benson, 1959; Aguilar-Armenta et al., 2001; Velisa, 2011; Liu et al., 2017).

**Table 3**Parameters for the apparent permeability ( $K_{app}$ ) model.

Parameters	Values	Data Sources
Average pore radius, $R_{avg}$	$3.6471 \times 10^{-9}$ m	Calculated from the initial matrix permeability (Table 1) by using the $K_{app}$ model and initial reservoir pressure
Temperature, $T$	410.15 K	BC Oil and Gas Commission, 2014
Tortuosity, $\tau$	2.5	Assumed
Fractal dimension of pore surface, $D_f$	2.5	Assumed
Universal gas constant, $R$	8.3144621 J/mol/K	Universal constant
Boltzmann constant, $B$	$1.38064852 \times 10^{-23}$	Universal constant
Molar mass of methane, $M$	$1.604 \times 10^{-2}$ kg/mol	Universal constant
Molecule diameter of methane, $R_{methane}$	$3.8 \times 10^{-10}$ m	Aguilar-Armenta et al., 2001
Collision diameter of methane, $R_{methane}$	$3.82 \times 10^{-10}$ m	Prausnitz and Benson, 1959
Critical pressure of methane, $P_{critical\ methane}$	$4.5992 \times 10^6$ Pa	Velisa, 2011
Critical temperature of methane, $T_{critical}$	190.564 K	Velisa, 2011

The effects of  $P$  and  $R_{avg}$  are illustrated in Figure 4 (a) and (b), where  $K_{app}$  is inversely proportional to  $P$  and directly proportional to  $R_{avg}$ . This sensitivity analysis illustrates the significance of incorporating a pressure-dependent  $K_{app}$  model in reservoir simulation for capturing the variability of gas permeability in shale gas production performance.

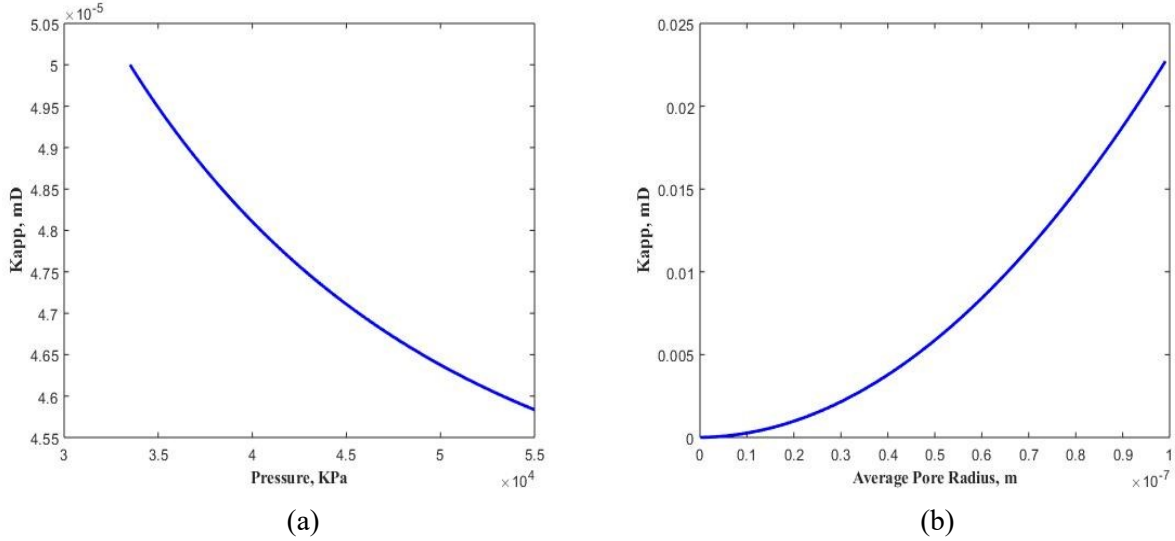


Figure 4.  $K_{app}$  as functions of (a) pressure and (b) average pore radius (examples).

### 3.3.2 Dynamic Updating of Apparent Permeability

To facilitate the dynamic updating of apparent permeability ( $K_{app}$ ), a novel explicit coupling scheme is formulated, as shown in Figure 5. To achieve a balance between computational efficiency and model accuracy, the  $K_{app}$  is updated periodically: at each updating time step, matrix pressures at the grid blocks are extracted from the flow simulator and a “restart” file is created; the  $K_{app}$  at each cell is then updated according to Eqs. 2-7 and returned to the simulator; the computation continues until the next updating step. The coupling code is implemented in MATLAB® (MathWorks, 2019).

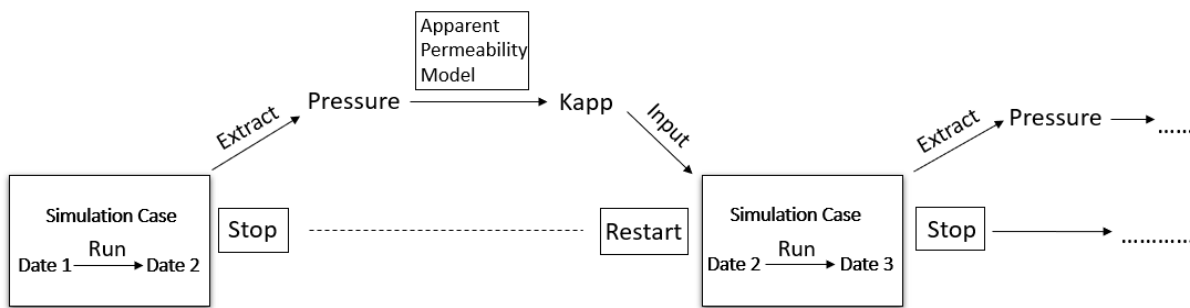


Figure 5. Coupling of  $K_{app}$  modeling and flow simulation.

The sensitivity of updating frequency is analyzed and presented in Figure 6. It is clear that there is essentially no improvement for updating more frequently than 10 days; therefore, an updating frequency of every 7 production days is selected in consideration of both simulation accuracy and computational efficiency.

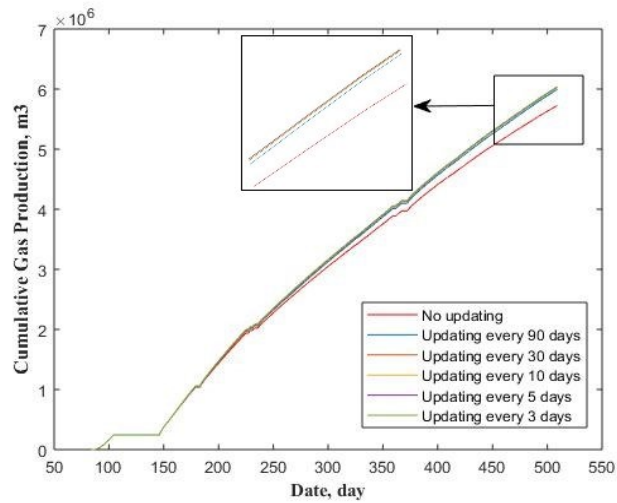


Figure 6. Cumulative gas production for different updating frequencies (examples).

## **Chapter 4: Impacts of Secondary Fracture Network and $K_{app}$**

### **Modeling**

In this chapter, our numerical model is calibrated from the field data of a well to examine the impacts of secondary fracture network and apparent permeability modeling on gas production and fracturing fluid recovery; the sensitivity analysis of secondary fracture intensity, the effects of reservoir pressure on apparent permeability modeling, matrix multiphase flow functions is discussed.

#### **4.1. Example with Field Production Data**

A base case is constructed by coupling both  $K_{app}$  and DFN modeling. The hydraulic fracture length is adjusted by history matching the field production data gathered from a well drilled in the Otter Park member of the Horn River Basin (B-G18-I/94-0-08), as presented in Liu et al. (2019). This well is selected because there is less observable inter-well interference (Yousefzadeh et al. 2016). There are 20 single-perforation stages of hydraulic fracturing with an average fracture spacing of 100 m, and a total of 75,504 cubic meters of fracturing fluid was injected over the 20 stages. The well was soaked for 84 days prior to flowback (Xu et al. 2016), and it was produced for 383 days. Results of the history matching are illustrated in Figure 7 (a).

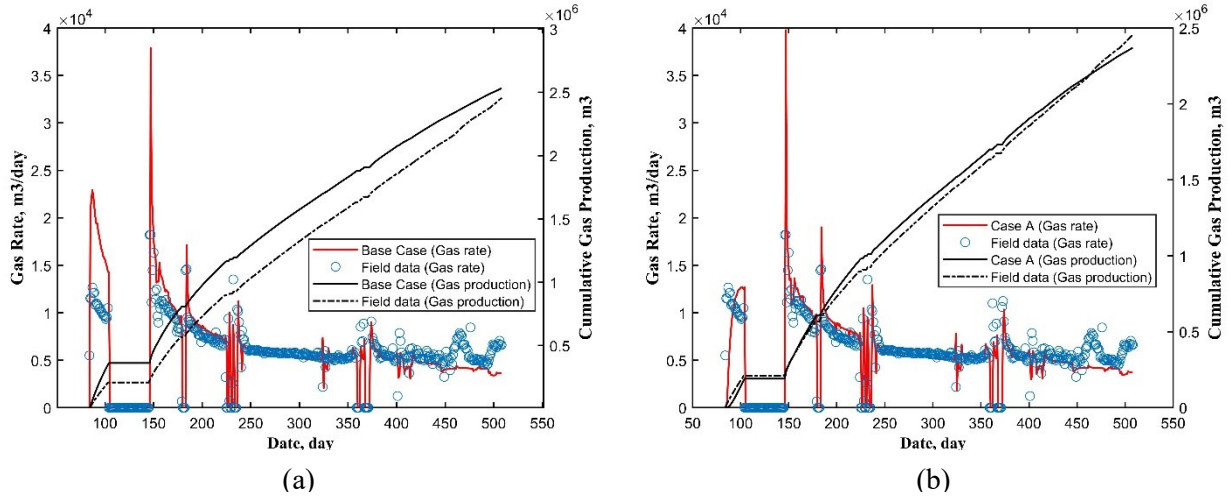


Figure 7. Comparison of production profiles between the field historical data and (a) Base Case and (b) Case A.

A reasonable match ( $< 3\%$  mismatch) is obtained in terms of cumulative production; the history-matching results have yielded an effective hydraulic fracture half-length of 83.00 m for the Base Case. A slightly larger mismatch is observed at the beginning of the flow-back process; a plausible explanation is that the estimated bottom-hole pressures during flow-back could be inaccurate due to rapidly changing multiphase flow conditions (Liu et al. 2017). In addition, those extremely high gas production rates at the beginning and fluctuations at the end of the production history may be attributed to operational issues that are not captured in the daily-averaged surface casing pressure used in the bottom-hole pressure calculations (Liu et al. 2017).

An additional case, Case A (Table 4), is constructed such that  $K_{app}$  and secondary fracture networks modeling are neglected. To match the same production history as the Base Case, the half-length of the hydraulic fracture is increased to 168.80 m. This result illustrates how neglecting the contributions due to  $K_{app}$  and secondary fractures in the simulation could overestimate the size of the hydraulic fracture for a given observed gas production. Results of the history matching for Case A are presented in Figure 7 (b).

**Table 4**

Summary of the cases studied.

Names	Remarks	Hydraulic fracture half lengths	Mismatches in cumulative gas production
Base Case	DFN + $K_{app}$ ( <i>History matched with field data</i> )	83.00 m	< 2.98%
Case A	DFN + $K_{app}$ modeling are ignored ( <i>History matched with field data</i> )	168.80 m	< 3.40%
Case B	Case A + DFN	168.80 m	-
Case C	Case A + $K_{app}$	168.80 m	-
Case D	DFN + $K_{app}$ + Secondary fracture closure ( <i>History matched with field data</i> )	93.73 m	< 3.11%
Case E	History-matched Case D without the secondary fracture closure	93.73 m	-

## 4.2. Impacts of Secondary Fracture Network

To further examine the effects of secondary fracture network modeling, Case B (Table 4) is constructed by incorporating DFN only: it can be viewed as adding the DFN effects to Case A (section 4.1). The gas production and water recovery profiles of Case B are compared with those corresponding to Case A in Figure 8 (a) and (b), respectively. As expected, improved overall conductivity due to the secondary fracture modeling has led to an increase in gas production. However, a huge reduction in water recovery is also observed, as more water could be transported further away from the wellbore. The results are consistent with those observed in previous studies (Wang and Leung, 2015a, b).

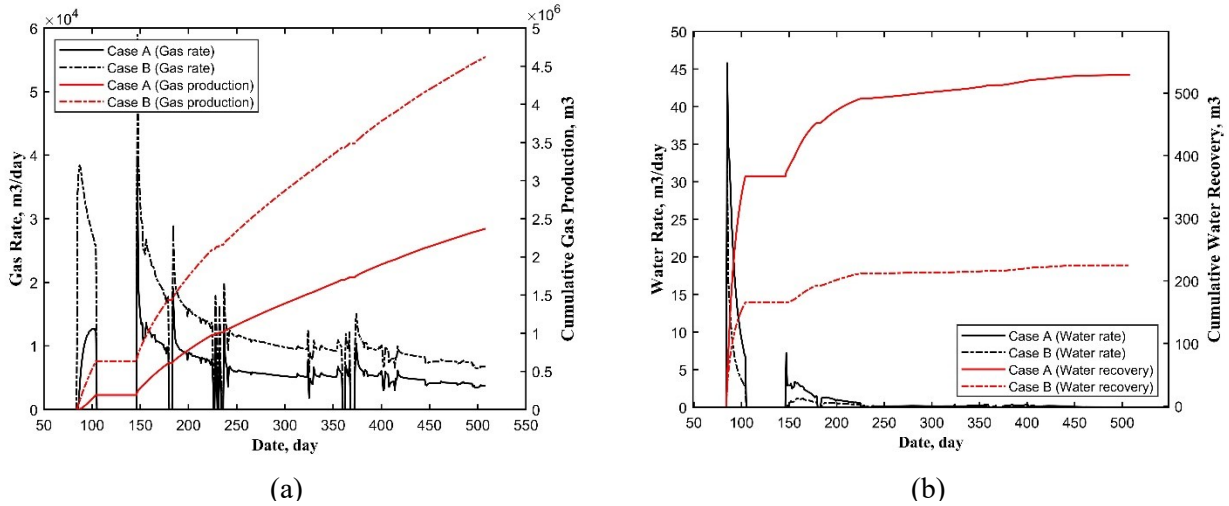


Figure 8. Profiles of (a) gas production and (b) water recovery for Case A and Case B.

Water saturation profiles in four specific regions in the fracture and matrix domains are systematically investigated (Figure 9 and Figure 10) to examine the fluid distribution. The presence of secondary fracture network has facilitated the imbibed water to flow further into the matrix and away from the hydraulic fracture (HF). During the soaking period, the secondary fractures in Case B has enabled more water from the HF to advance further into matrix; therefore, the  $S_w$  (water saturation) is lower in regions 1 and 2, and higher in regions 3 and 4, in comparison to that for Case A. It is interesting to note in Figure 10 (d) that without secondary fractures, water saturation in region 4 remains unchanged (Case A) – but a slight increase is observed for Case B. Due to the ultra-low conductivity of the matrix, once the water has imbibed deep into the matrix, it would be very difficult for that water to be flown back, as corroborated by a reduced water recovery for Case B in Figure 8 (b). This also explains why a higher  $S_w$  is observed in both regions 3 and 4 for Case B during the whole production period, as shown in Figure 10 (c) and (d).

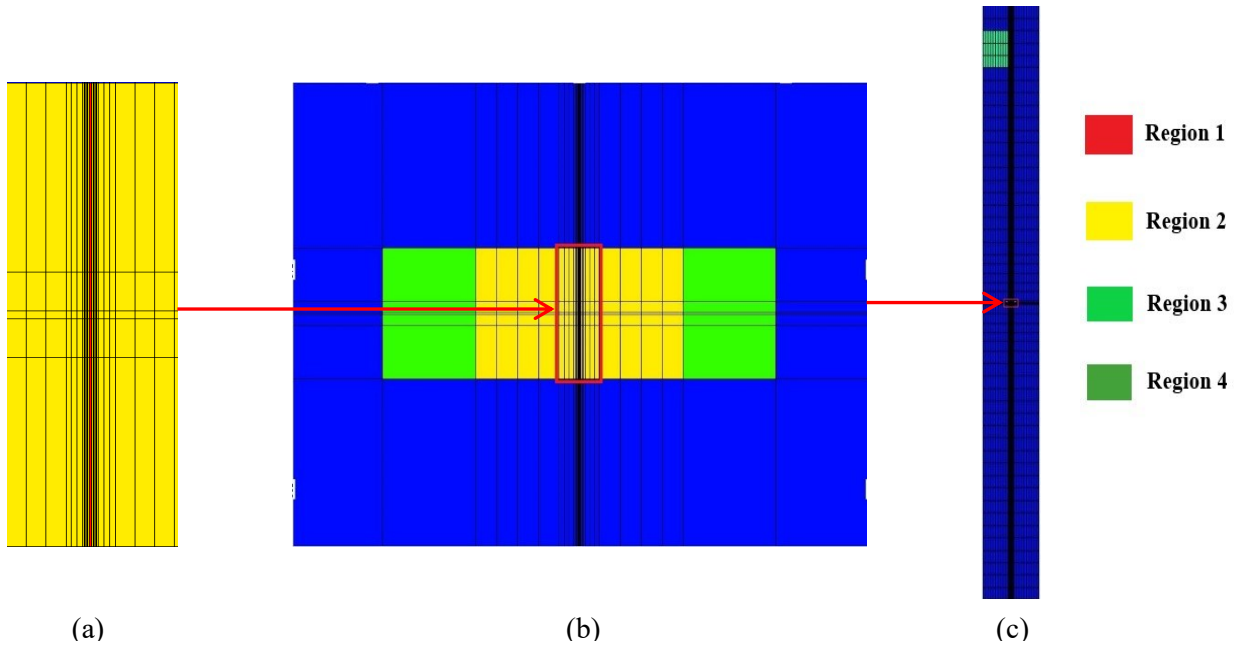


Figure 9. Top view of the four regions selected for fluid-loss investigation [Region 1: inside HF; Region 2: matrix immediately adjacent to HF; Region 3: matrix in the near-well region (but not immediately adjacent to the HF); Region 4: matrix far away from HF].

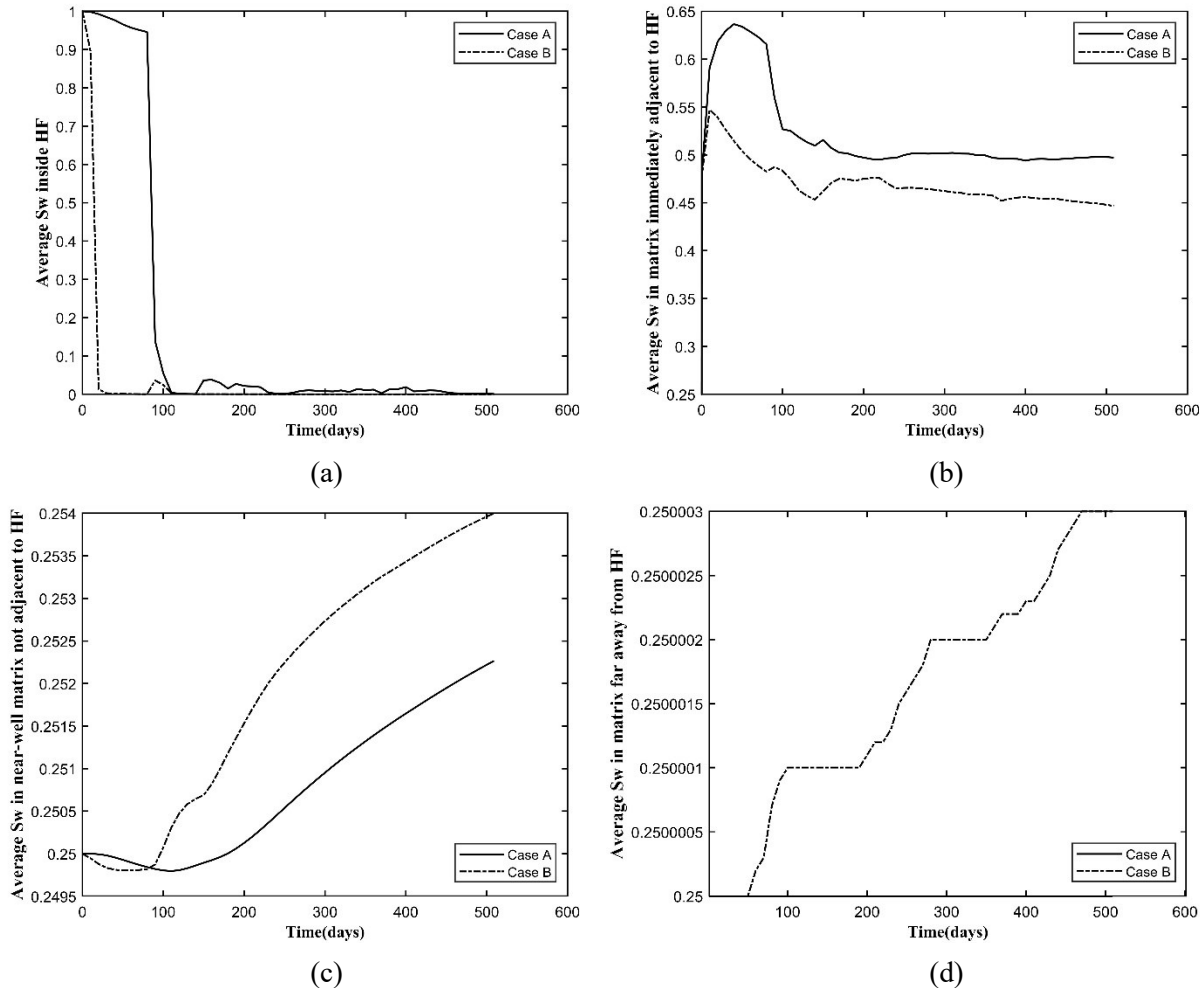


Figure 10. Effects of DFN modeling on average water saturation profiles: (a) Region 1, (b) Region 2, (c) Region 3, (d) Region 4.

### 4.3. Impacts of Apparent Permeability Modeling

To further examine the effects of  $K_{app}$  modeling, Case C (Table 4) is constructed by incorporating  $K_{app}$  modeling only: it can be viewed as adding the  $K_{app}$  modeling to Case A (section 4.1). The gas production and water recovery profiles of Case C are compared with those corresponding to Case A, as shown in Figure 11 (a) and (b), respectively. Similar to Case B (section 4.2), enhanced matrix permeability has resulted in an increase in gas production, while a reduction in water recovery is also observed.

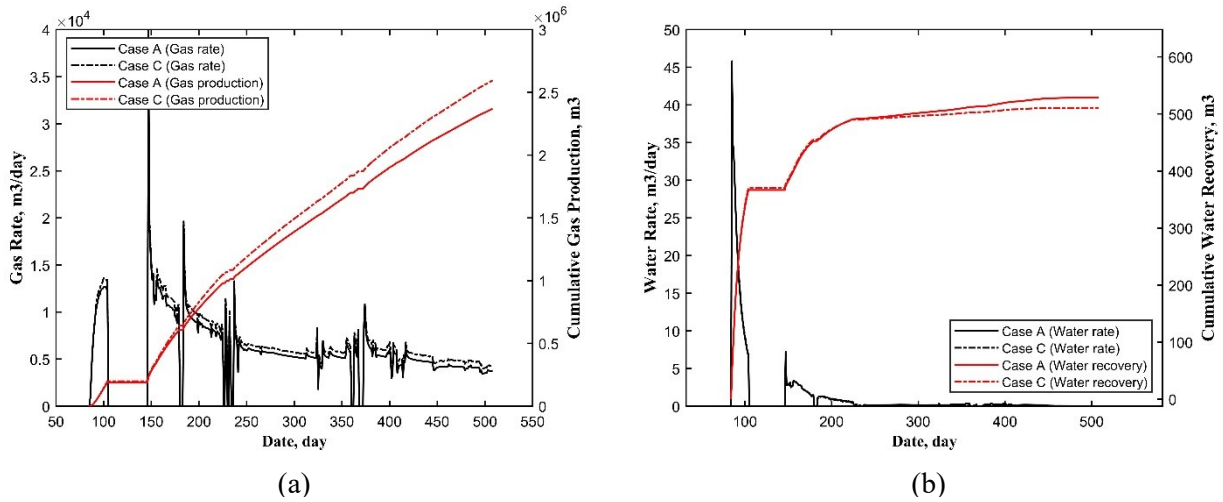


Figure 11. Profiles of (a) gas production and (b) water recovery for Case A and Case C.

Water saturation profiles in the four specific regions (same as those defined in section 4.2) are examined, as shown in Figure 12. Incorporating  $K_{app}$  seems to have negligible impact on fluids distribution: identical water profiles are observed in the four regions during the soaking period ( $< 84$  days); this is because the pressure gradient remains low before the well is opened; the same reasoning would also explain why essentially no water has imbibed deep into region 4. However, during the production period ( $t > 84$  days), a slightly higher water saturation is observed in regions 2 and 3 in the case with  $K_{app}$  modeled. This is likely due to the water expanding while more gas is being produced (corroborated by the increase in gas production and gas rate during production period) when incorporating of the multiple non-Darcy gas flow mechanisms in the reservoir modeling.

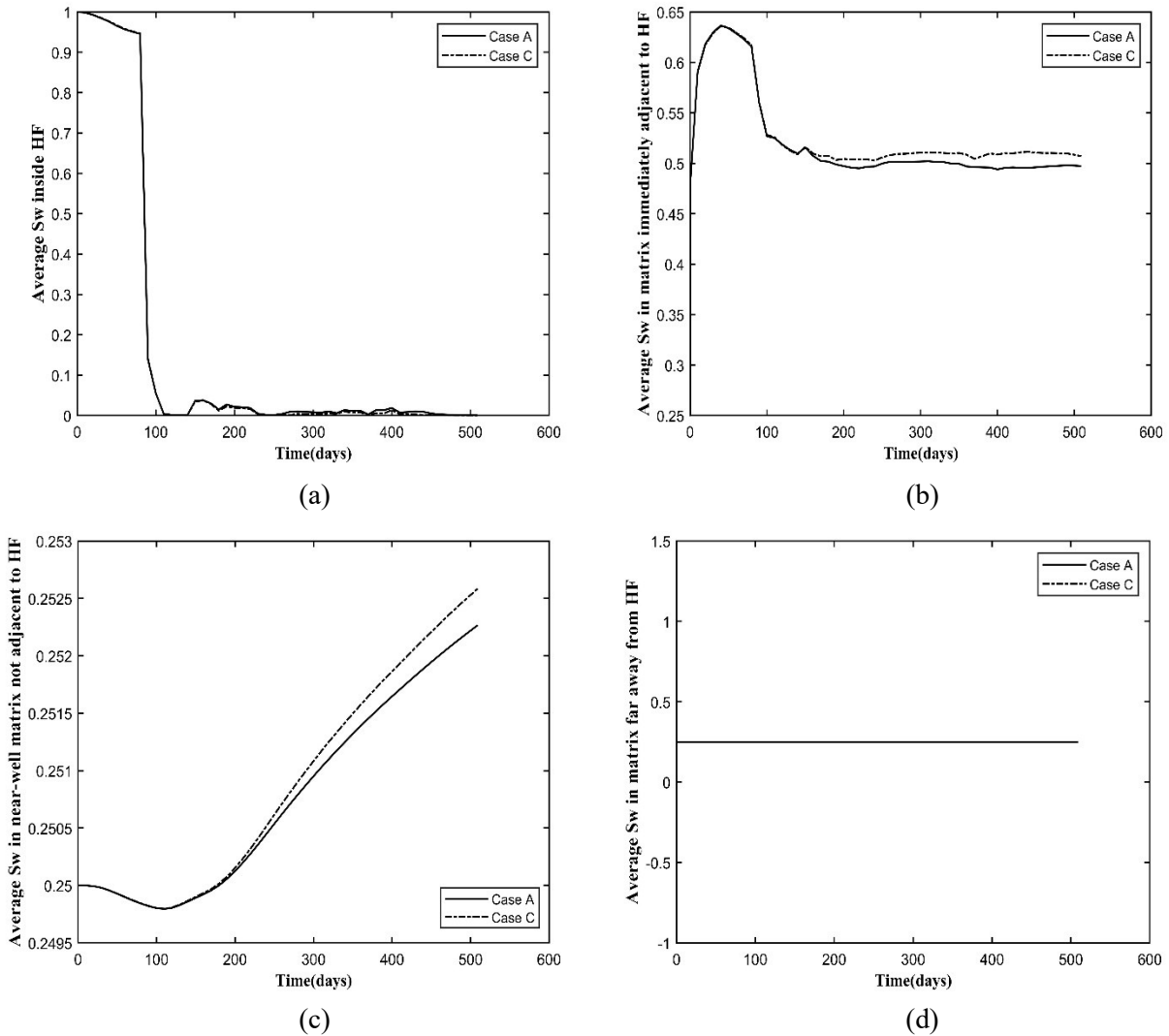


Figure 12. Effects of  $K_{app}$  modeling on average water saturation profiles: (a) Region 1, (b) Region 2, (c) Region 3, (d) Region 4.

## 4.4. Sensitivity Analysis

### 4.4.1 Effects of Secondary Fracture Intensity

Case B illustrated the effects of secondary fracture. In this section, sensitivity of fracturing fluid recovery due to fracture intensity is assessed. Case 1 with a fracture intensity value of 0.0138 1/ft, which is twice the Base Case's value, is constructed. The comparisons are presented in Figure 13,

where similar trends as those of Case B (Figure 8 and Figure 10) can be inferred, except that the effects of secondary fractures are further exaggerated (particularly in region 4, as shown in Figure 13b). This notable difference is contrary to conclusions obtained in previous studies involving oil-water systems, which seem to suggest that there would be no improvement of long-term water recovery from denser fracture networks (Wang and Leung, 2015a, b).

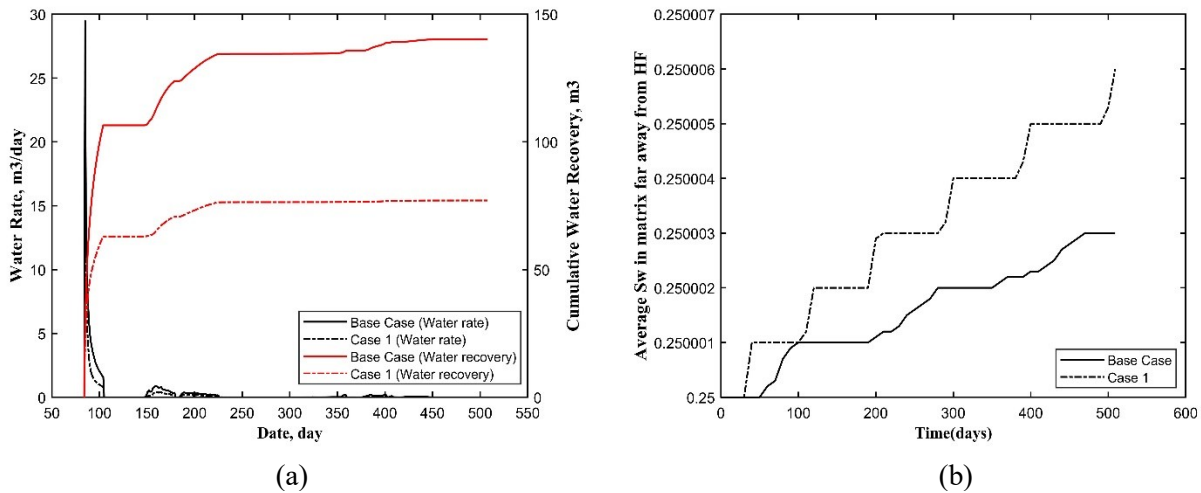


Figure 13. DFN models with different levels of fracture intensity: (a) water recovery, (b) average water saturation in region 4.

#### 4.4.2 Effects of Reservoir Pressure and $K_{app}$

Three pairs of cases are tested: ‘Base Case’ and ‘Base Case (No  $K_{app}$ )’, ‘Case 2’ and ‘Case 2 (No  $K_{app}$ )’, ‘Case 3’ and ‘Case 3 (No  $K_{app}$ )’. Three initial reservoir pressures: 34,000 kPa (the same as Table 1), 53,500 kPa and 13,500 kPa, are assigned to these three sets of cases, respectively. The corresponding gas and water production profiles are compared in Figure 14.

As expected, higher gas and water production is observed, as the initial reservoir pressure increases; this can be explained by an increase in the initial gas-in-place and larger draw-down.

As discussed in section 4.3, enhanced matrix permeability due to the incorporation of  $K_{app}$  has resulted in an increase in gas production. As shown in Figure 14, for the three initial reservoir pressures of 53,500 kPa, 34,000 kPa and 13,500 kPa, increases in gas production of 2.19%, 4.30% and 12.00%, are recorded respectively – the impact of  $K_{app}$  modeling is more noticeable at lower initial reservoir pressure. This is because there are fewer collisions between the gas molecules at low pressures, and the gas mean free path would increase; as a result, the effects of the interactions between the molecules and the solid surface become more significant, rendering the nano-pore flow mechanisms, such as Knudsen diffusion, to be more dominant. It is interesting to note that, at very high reservoir pressure (e.g., the case with 53,500 kPa), enhancing matrix permeability due to  $K_{app}$  modeling would increase water recovery (opposite to the results in section 4.3). A plausible explanation is that when the matrix pressure is very high, there is little pressure gradient between the HF and matrix, reducing the amount of water flowing from the HF into the matrix, so more water can be recovered.

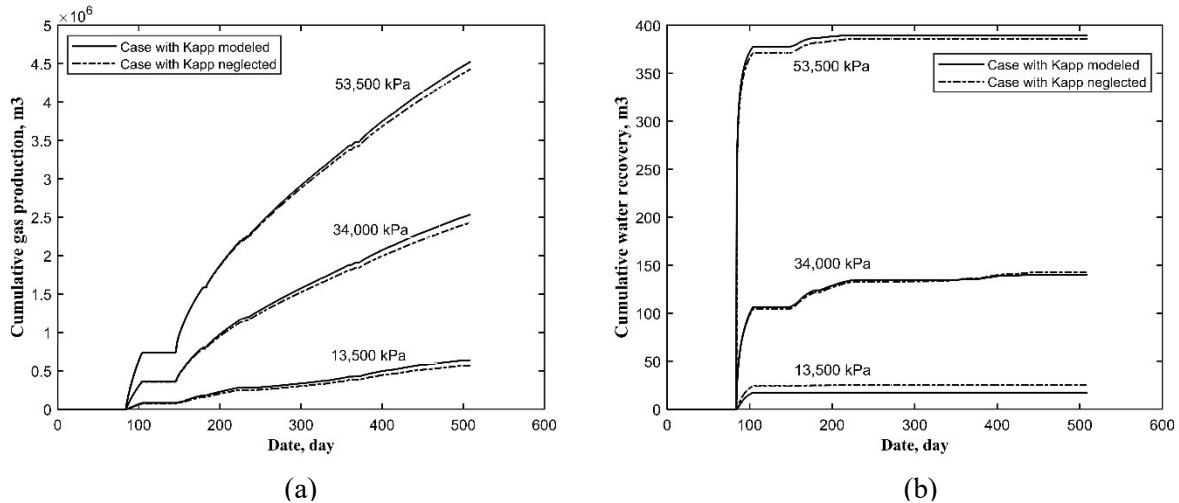


Figure 14. (a) Cumulative gas production and (b) water recovery for the three pairs of cases with different initial reservoir pressure.

### 4.4.3 Effects of Matrix Capillary Pressure ( $P_c$ )

Cases 4 and 5 with the following water/gas capillary pressure functions are examined, as plotted in Figure 15 (a):  $P_{c \text{ Base Case}} > P_{c \text{ Case 4}} > P_{c \text{ Case 5}}$ . Modeling of secondary fracture closure is neglected in all three cases. The corresponding gas and water production profiles are compared in Figure 15 (b), while the water volumes in the four specified regions (see section 4.2) are compared in Figure 16.

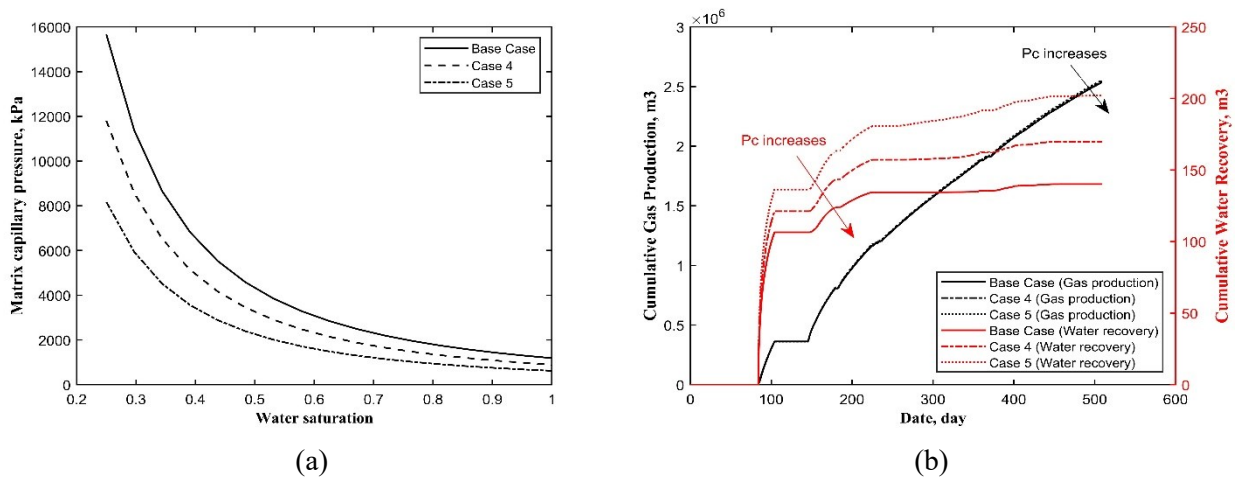


Figure 15. (a) Capillary pressure functions and (b) the corresponding cumulative gas production and water recovery profiles.

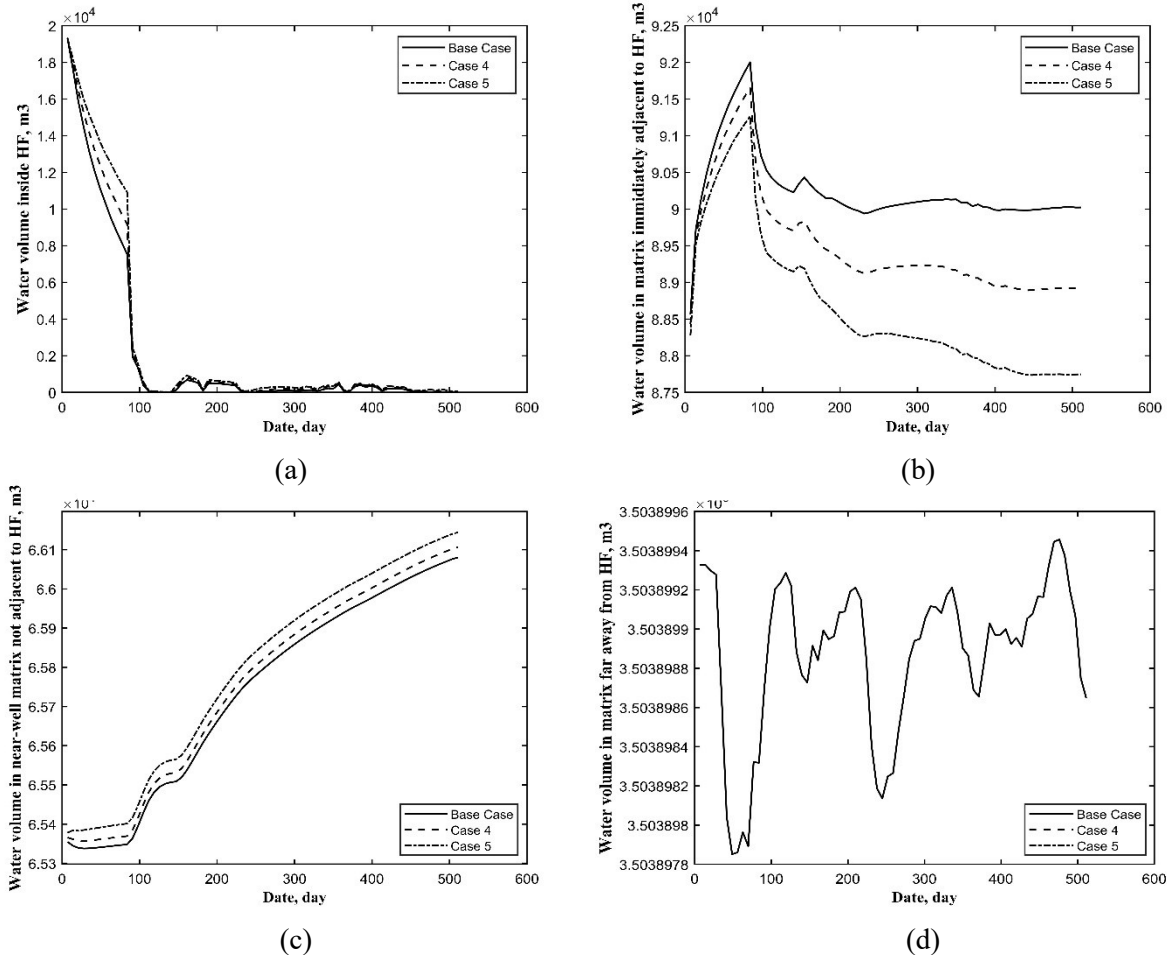


Figure 16. Effects of matrix capillary pressure on water volumes in: (a) Region 1, (b) Region 2, (c) Region 3, (d) Region 4.

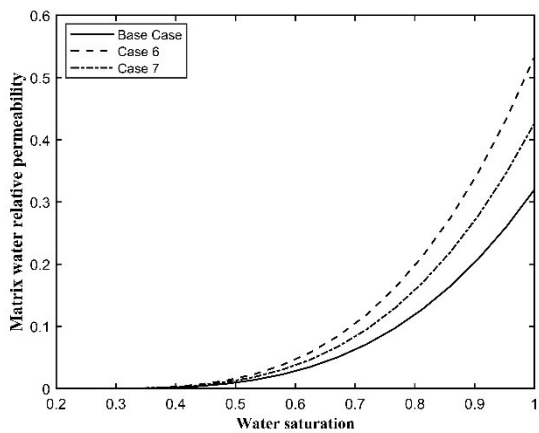
During the soaking period ( $t < 84$  days), higher  $P_c$  leads to an increased water flow from the HF to the matrix due to imbibition, and this is corroborated by a more dramatic decrease of water volume in region 1 corresponding to an increase in  $P_c$ . The additional imbibed water leads to more water in region 2. On the other hand, less water is observed in region 3 for the case with higher  $P_c$ ; this is because much of the imbibed water remains in region 2 due to the strong capillary force, and, as a result, less water would advance into regions 3 and 4. This also explains why the water volumes observed in region 4 are essentially identical. During the production period ( $t > 84$  days), generally speaking, less water is recovered with an increase in matrix  $P_c$ : water that is accumulated

in region 1 is produced, irrespective of the  $P_c$  level, while more water is retained in areas away from region 1 due to the stronger capillary force.

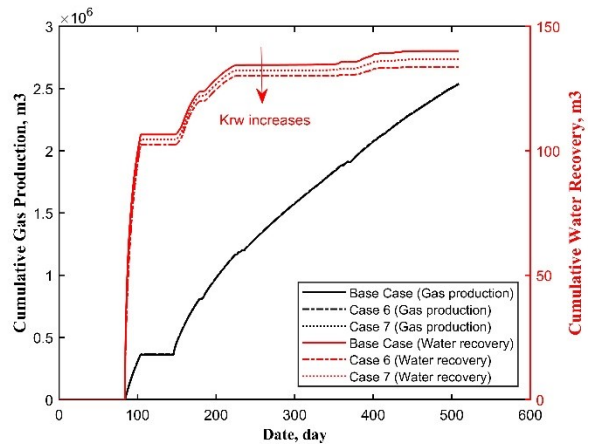
Interestingly, previous studies involving water-oil systems have concluded that stronger matrix imbibition leads to higher initial oil rate, with more oil being displaced into the fractures and be produced, although no long-term benefits in oil production was reported (Wang and Leung, 2015a, b); however, in this water-gas system, the gas production actually slightly decreases with matrix  $P_c$ , as shown in Figure 15 (b). The reasons are (1) considering gas is much more compressible than water, less gas is being displaced from the matrix (i.e., region 2) into the HF as a result of countercurrent imbibition during the soaking period; (2) higher water retention in region 2 for cases with higher  $P_c$  (Figure 16) would actually hinder gas production due to reduction in gas relative permeability.

#### **4.4.4 Effects of Matrix Water Relative Permeability ( $K_{rw}$ )**

Cases 6 and 7 with the following water relative permeability functions, as plotted in Figure 17 (a), are examined:  $K_{rw \text{ Case } 6} > K_{rw \text{ Case } 7} > K_{rw \text{ Base Case}}$ . Modeling of secondary fracture closure is neglected in all three cases. The corresponding gas and water production profiles are compared in Figure 17 (b), while the water volumes in the four specified regions (see section 4.2) are compared in Figure 18.

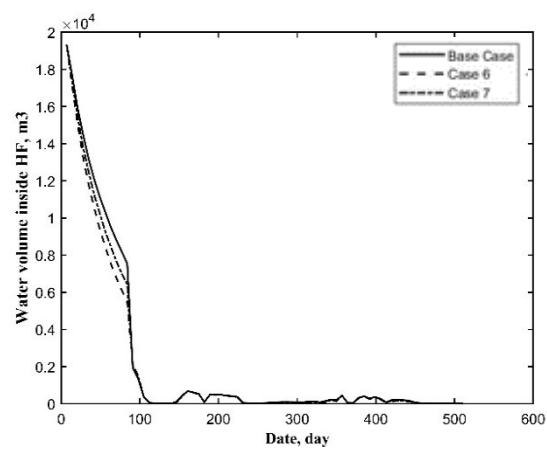


(a)

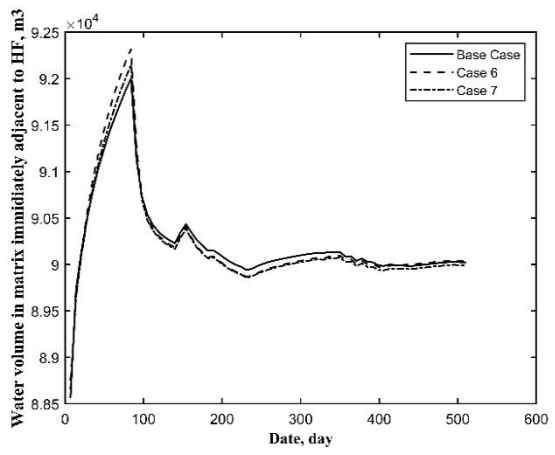


(b)

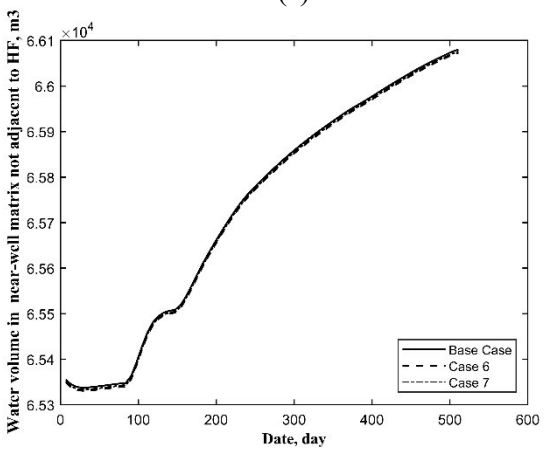
Figure 17. (a) Water relative permeability functions and (b) the corresponding cumulative gas production and water recovery.



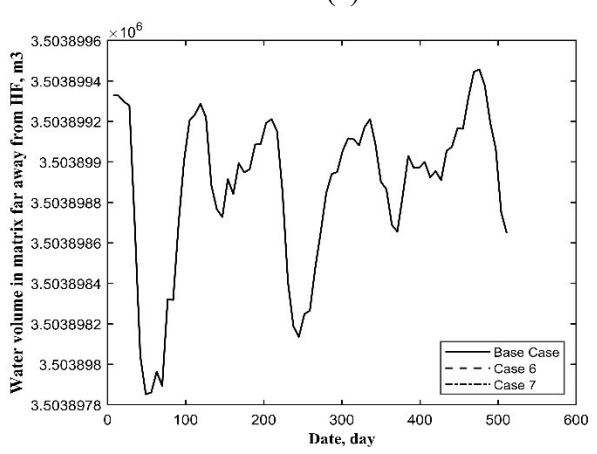
(a)



(b)



(c)



(d)

Figure 18. Effects of matrix water relative permeability on water volumes in: (a) Region 1, (b) Region 2, (c) Region 3, (d) Region 4.

During the soaking period ( $t < 84$  days), higher  $K_{rw}$  leads to increased water flow from the HF to the matrix, and this is corroborated by a more dramatic decrease of water volume in region 1, as well as a more dramatic increase of water volume in region 2. Given that a larger volume of water is firstly imbibed in region 2 for a higher  $K_{rw}$ , the water volume could be imbibed into regions 3 and 4 is minimal. As more water is imbibed in the near-well matrix and less water is retained in the secondary fractures, less water is produced during the flowback and production period.

There is no observable difference in gas production among the three cases with different matrix  $K_{rw}$ . As explained earlier (see section 4.4.3), little gas is being displaced from the matrix into the HF as a result of countercurrent imbibition during the soaking period. In the end, increasing matrix  $K_{rw}$  has insignificant impacts on the gas production.

#### **4.4.5 Effects of Matrix Gas Relative Permeability ( $K_{rg}$ )**

Cases 8 and 9 with the following gas relative permeability functions, as plotted in Figure 19 (a), are examined:  $K_{rg \text{ Base Case}} > K_{rg \text{ Case 8}} > K_{rg \text{ Case 9}}$ . Modeling of secondary fracture closure is neglected in all three cases. The corresponding gas and water production profiles are compared in Figure 19 (b), and the water volumes in the four specified regions (see section 4.2) are compared in Figure 20.

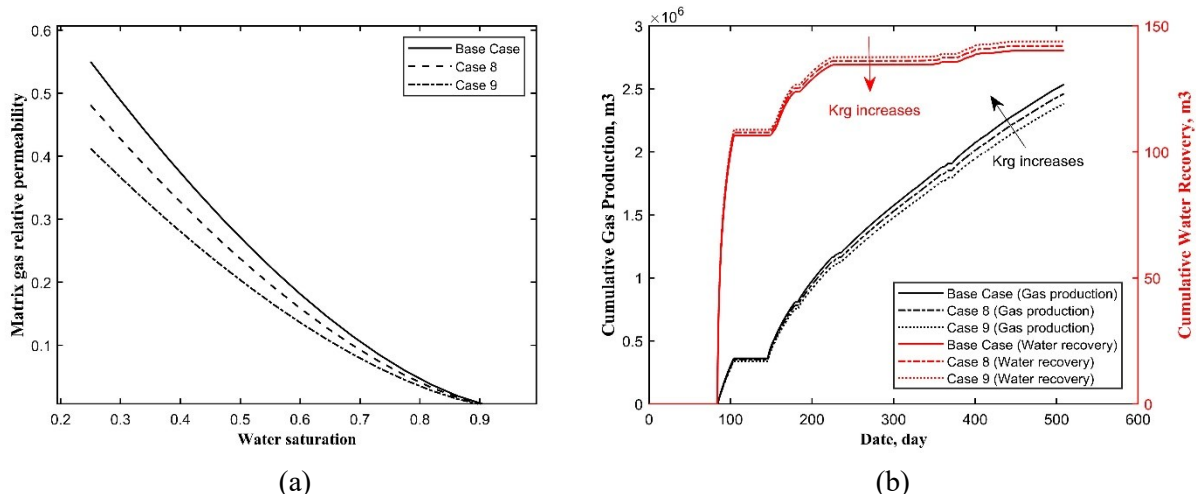


Figure 19. (a) Gas relative permeability functions and (b) the corresponding cumulative gas production and water recovery profiles.

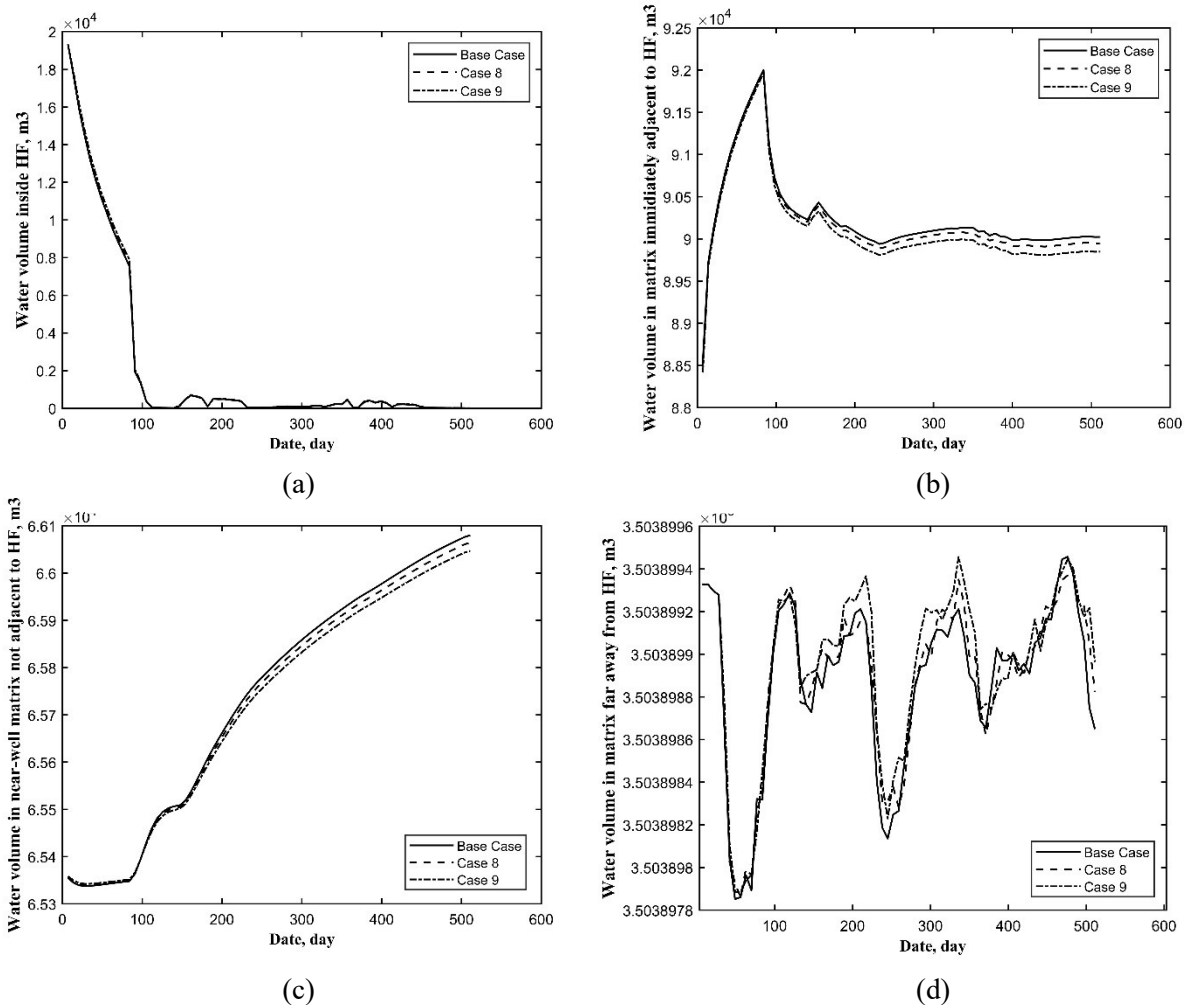


Figure 20. Effects of matrix gas relative permeability on average water saturation profiles: (a) Region 1, (b) Region 2, (c) Region 3, (d) Region 4.

Generally speaking, higher matrix  $K_{rg}$  would enhance gas flow from the matrix. Effects on water imbibition into the matrix during the soaking period ( $t < 84$  days) is negligible in all four regions. However, during the production period ( $t > 84$  days), a slightly larger water volume is observed in regions 2 and 3 with an increase in  $K_{rg}$ . This is likely due to reduced relative mobility for the water phase as  $K_{rg}$  increases. Once again, it is difficult to produce the additional water volumes from regions 2 and 3 due to the low water mobility. This is contrary to findings in previous studies involving oil-water systems where negligible influence of  $K_{rg}$  on water recovery was recorded (Wang & Leung, 2015a, b).

## **Chapter 5: Impacts of Secondary Fracture Closure**

In this chapter, the methodology used for integrating the dynamic closure process of secondary fractures is introduced; the impacts of secondary fracture closure on gas production and fracturing fluid recovery are discussed; the sensitivities of multiphase flow functions and shut-in durations for the cases incorporating secondary fracture closure are analyzed.

### **5.1 Modeling of Secondary Fracture Closure Using Rock-Type Indicators**

As a fracture cell is closed due to an increase in effective stress, it is anticipated that the corresponding porosity and permeability would become zero. This modeling idea can be facilitated with the use of “rock types” – the keyword “CTYPE” for assigning “compressibility, compaction and dilation rock types to reservoir grid blocks” (CMG, 2016). Two rock types are designated to represent the open and the closed states. A look-up table of porosity and permeability multipliers versus pressure is provided in each rock type. In the case of complete fracture closure, the porosity multiplier (i.e., ratio of pore volume measured at a given pressure to the initial pore volume), as well as the horizontal or vertical permeability multiplier (i.e., ratio of horizontal or vertical permeability measured at a given pressure to the initial horizontal permeability), are all set to 0. In the case of open fractures, the porosity multiplier is assigned to be close to 1, with a very slight decrease corresponding to the decreasing reservoir pressure; the horizontal or vertical permeability multipliers are assigned to follow an exponential relationship with the reservoir pressure, which was obtained from Nejadi et al. (2015), to model the normal compaction or dilation of an open secondary fracture.

At the beginning, all secondary fracture cells (in the DPDK model) are set as *open*; as the simulation progresses, some cells would be *closed* due to changes in effective stress conditions. An explicit coupling scheme is implemented to facilitate the simulation of this dynamic closure process, as shown in Figure 21. At each time step of updating, secondary fracture pressure values are extracted from the flow simulator and a “restart” file is created. If the fracture pressure is lower than the closure stress of complete fracture closure, which is assumed to be 18,000 kPa for the Horn River shale reservoirs (Beaudoin et al., 2011), the “rock type” corresponding to that particular cell is updated to *closed*; otherwise, it remains as *open*. The computation continues until the next updating step. The code is implemented in MATLAB® (MathWorks, 2019). Both  $K_{app}$  and secondary fracture rock types are updated simultaneously every 7 producing days after soaking period.

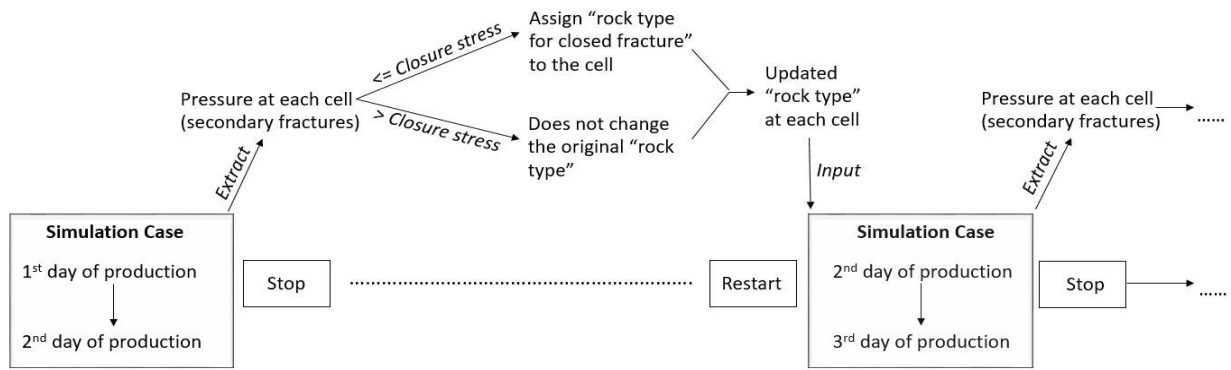


Figure 21. Coupling of secondary fracture closure modeling and flow simulation.

## 5.2 Impacts of Secondary Fracture Closure on Fracturing Fluid Recovery

Case D (Table 4) is the same as the Base Case, except for that secondary fracture closure is considered, and its production profiles are compared with the field data in Figure 22. Upon history-matching using the same field history as the Base Case, the hydraulic fracture half-length is

increased to 93.73 m. This value is approximately 10.73 m larger than that for the Base Case, implying that the size of hydraulic fracture is underestimated by 13% in the Base Case, where closure of secondary fracture is ignored. In other words, for a certain observed gas production, secondary fractures would contribute less to gas flow if some of them are closed due to changes in effective stress during production.

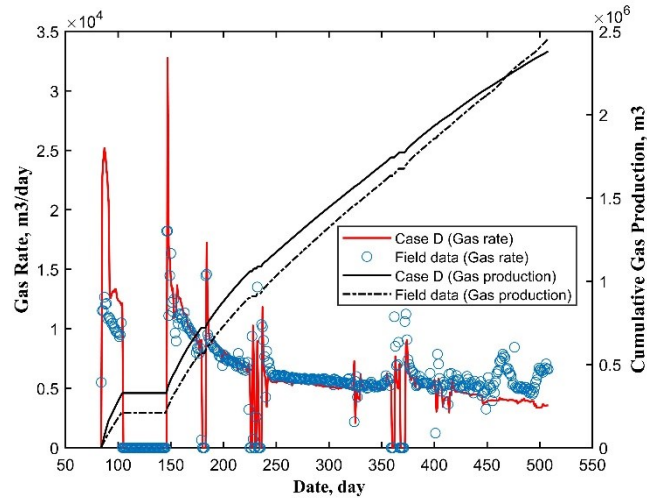


Figure 22. Comparison of production profiles between the field historical data and Case D.

Another case, Case E, is established using the history-matched hydraulic fracture half-length from Case D, but without accounting for the secondary fracture closure behavior. As shown in Figure 23, both gas production and water loss increase in Case E, as explained in the next section.

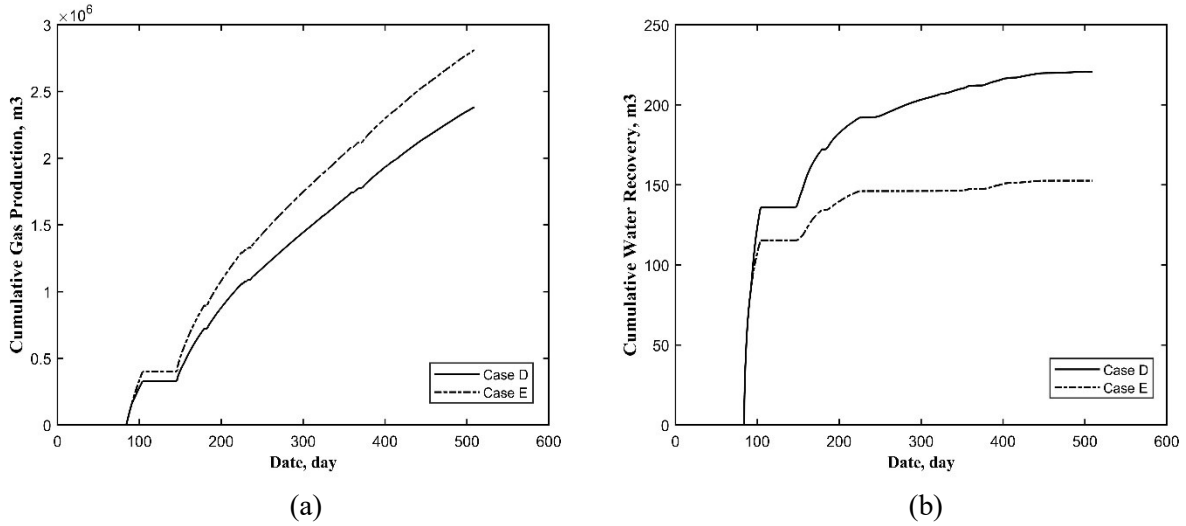
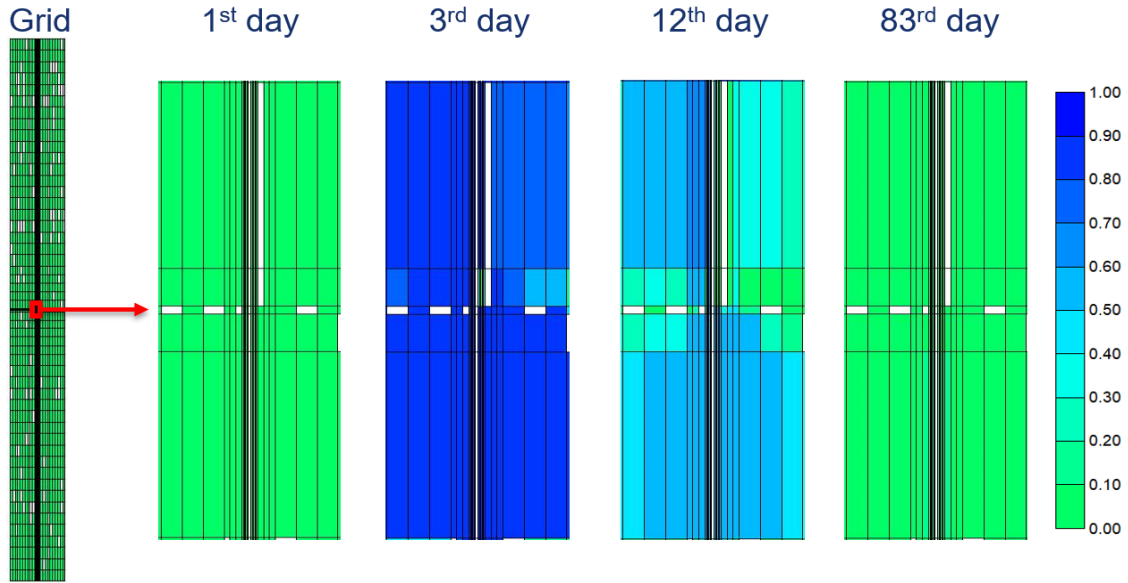


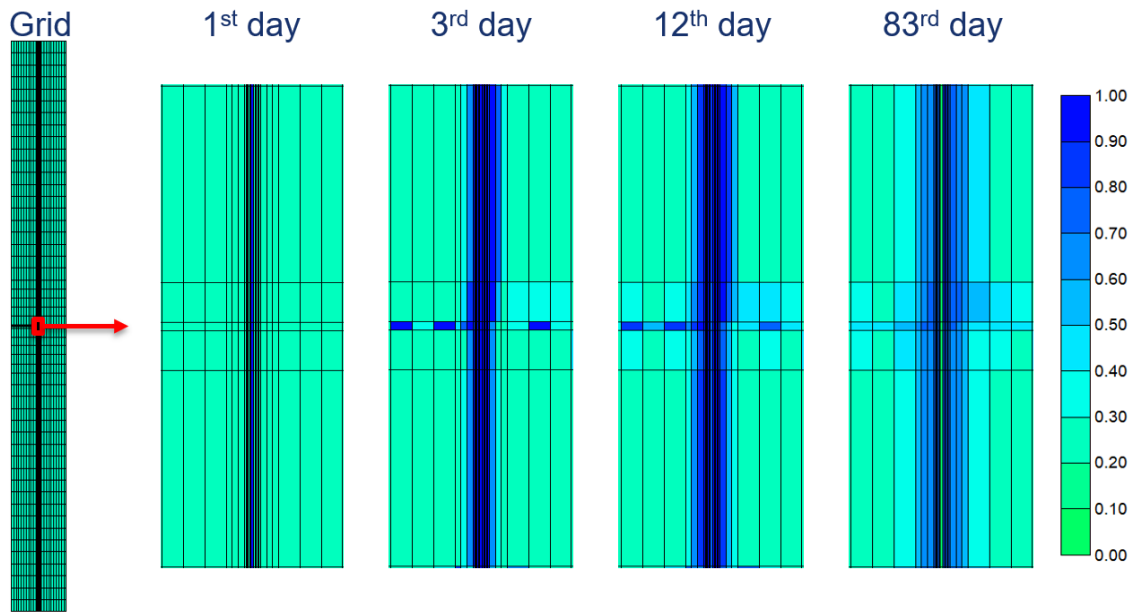
Figure 23. Comparison between Case D and Case E in terms of (a) gas production and (b) water recovery.

Results of Case D suggest that water retention in the formation may potentially hinder gas flow:

- 1) Upon shutting in the well during the soaking period, water in the hydraulic fracture would propagate to the connecting secondary fractures, the water would subsequently imbibe into it surrounding matrix due to counter-current imbibition, this is evidenced by the increase of water saturation at the beginning of the soaking period in the near-well secondary fractures and the subsequent decrease of water saturation, as shown in Figure 24 (a); this redistribution of fluids causes the matrix water saturation in the near-well region to increase, as shown in Figure 24 (b); gas flows into the secondary fractures that are connected to the hydraulic fracture due to the counter-current imbibition.



(a)



(b)

Figure 24. Top view of water saturation maps of (a) the near-well secondary fracture system and (b) matrix system at different dates in Case D.

- 2) Secondary fractures may close during flowback and production due to pressure depletion (Figure 25): as the secondary fractures adjacent to the hydraulic fracture close during flowback and early production, the fluids residing in the closing fractures would flow to the wellbore directly; however, during the later stage of production, more secondary fractures in areas away

from the wellbore begin to close, and the fluids residing in those closing fractures would not flow to the wellbore directly, as the flow paths are blocked by those previously closed fractures in the near-well areas; instead, the fluids would likely flow into the surrounding matrix, as a noticeable increase in water volume is detected in the surrounding matrix adjacent to the previously closed fracture. Change in gas volume, however, is less noticeable due to its compressibility.

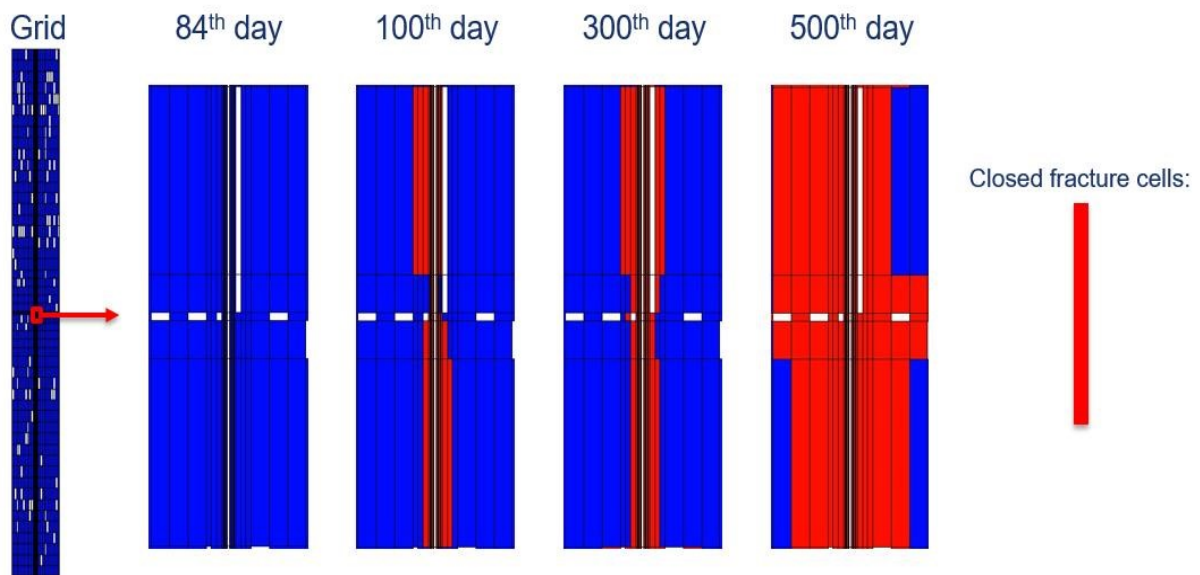
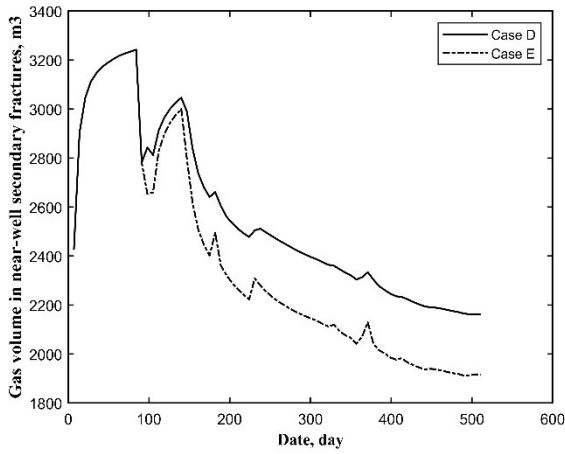


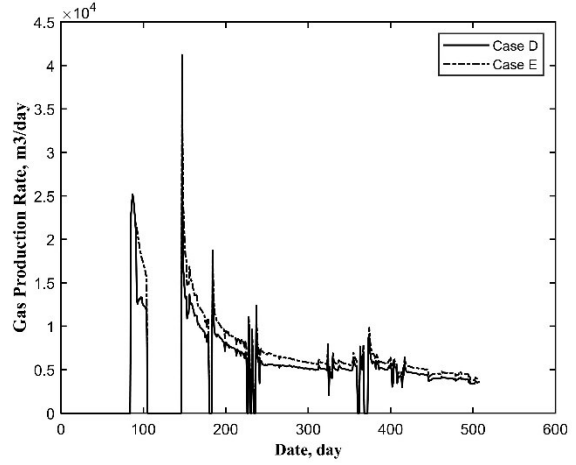
Figure 25. Top view of closed fracture cells in the near-well region at different production dates in Case D.

- 3) Due to the disconnection of secondary fractures, gas flow to the hydraulic fracture is primarily through the matrix. However, the large amount of water accumulated in the near-well region could potentially hinder gas flow to the well due to a reduction in gas relative permeability. Therefore, more gas is found in the remaining open secondary fractures (Figure 26a), while the gas production rate is much lower (Figure 26b). Interestingly, a reduction in water loss is also observed (Figure 26c, d). The only difference between Case E and the Case D is that secondary fracture closure is not considered in Case E. The reduction in gas production (due

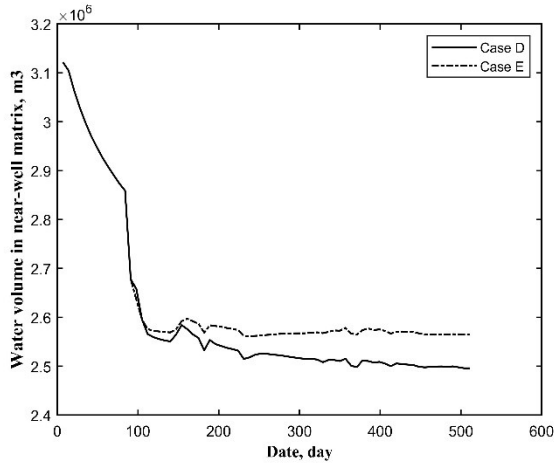
to secondary fracture closure in the Case D) has led to a higher matrix pressure (Figure 26e)  
– higher matrix pressure, coupled with water accumulation in the near-well region, would have contributed to an increase in water flow into the hydraulic fracture and water recovery (as evidenced by a higher water recovery rate observed in Figure 26d).



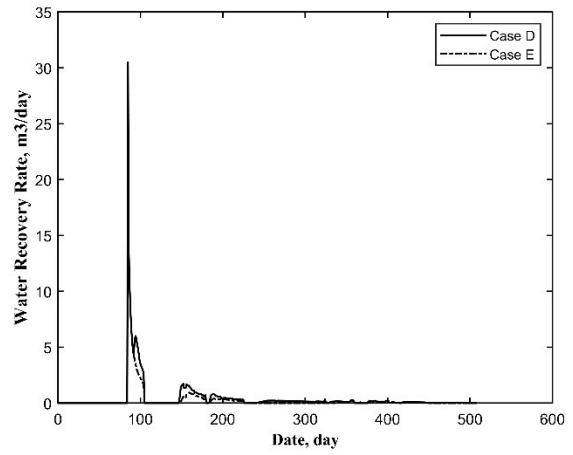
(a)



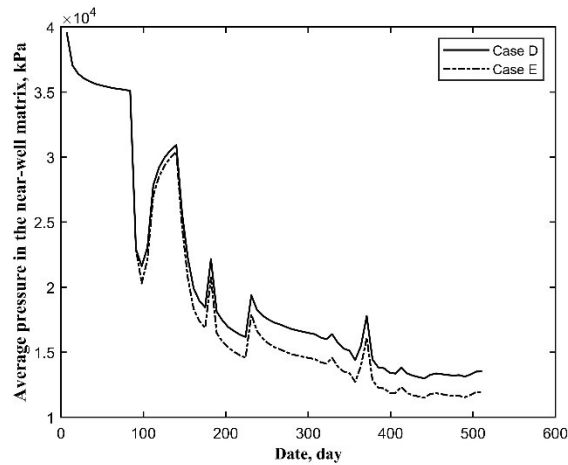
(b)



(c)



(d)



(e)

Figure 26. (a) Change in gas volume with time in the near-well secondary fracture; (b) gas production profiles of Case D and Case E; (c) change in water volume with time in the near-well matrix; (d) water production profiles of Case D and Case E; and (e) change in average matrix pressure in the near-well region.

## 5.3 Sensitivity Analysis (Secondary Fracture Closure Considered)

### 5.3.1 Effects of Matrix Capillary Pressure

To examine the sensitivity of matrix capillary pressure on recovery performance, Cases 10 and 11 with the following water/gas capillary pressure functions (the same as section 4.4.3) are examined:  $P_{c \text{ Case D}} > P_{c \text{ Case 10}} > P_{c \text{ Case 11}}$ . Secondary fracture closure is considered in all three cases. The corresponding gas profiles are compared with the Case D in Figure 27 (a). As  $P_c$  increases, more water would imbibe into the matrix and more gas would flow into the secondary fractures. As shown in Figure 27 (b), there is more gas in the near-well secondary fractures during the soaking period (initial 84 days) for Case D, and more gas is retained in the secondary fractures due to fracture closure during the production period as well. However, the additional gas volume remained in the open secondary fractures is limited (approximately a few hundred cubic meters). A more plausible explanation for the reduced gas production is the water blockage in the near-well matrix (Figure 27c). This observation is corroborated by the decrease in gas and water production for the Case D, as shown in Figure 27 (a). This finding is contrary to what was observed in previous studies where fracture closure was ignored; those studies observed that, for an oil-water system, enhanced imbibition might improve the initial oil rate, but no benefit regarding the long-term oil production was noted (Wang and Leung, 2015a, b).

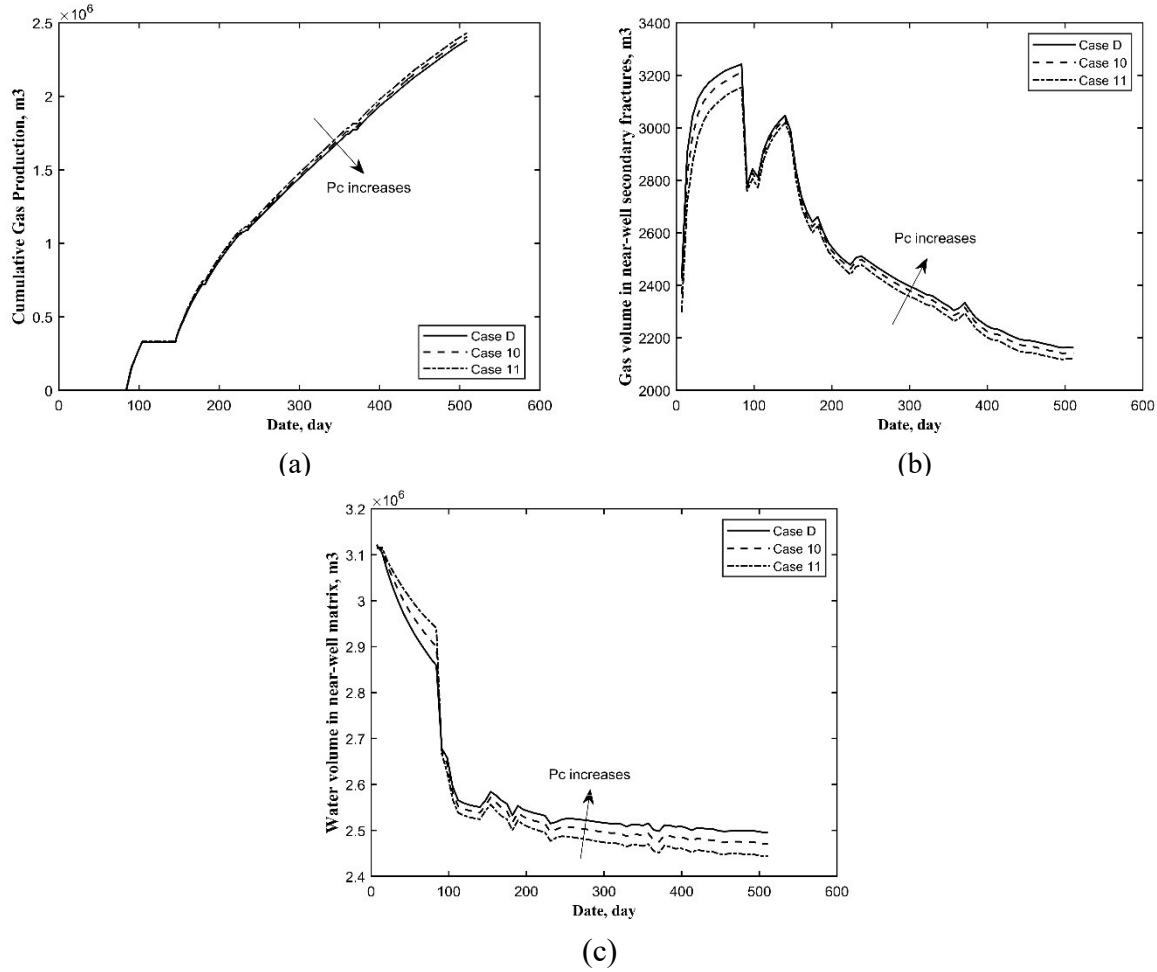


Figure 27. (a) Cumulative gas production; (b) gas volume in near-well secondary fractures; and (c) water volume in the near-well matrix corresponding to various matrix capillary pressure functions.

### 5.3.2 Effects of Matrix Water Relative Permeability

To examine the sensitivity of matrix water relative permeability on recovery performance, Cases 12 and 13 with the following water relative permeability functions (the same as section 4.4.4) are examined:  $K_{rw \text{ Case 12}} > K_{rw \text{ Case 13}} > K_{rw \text{ Case D}}$ . Secondary fracture closure is considered in all three cases. The corresponding water production profiles are compared with Case D in Figure 28 (a). There are almost no observable differences in water recovery profiles, this result is different from the water profiles obtained in section 4.4.4 where fracture closure is neglected (Figure 17b). If fracture closure is neglected, one would have expected that as  $K_{rw}$  increases, less water would

remain in the secondary fractures and be recovered (Wang and Leung, 2015a, b); however, if secondary fracture closure is considered, the water that is residing in the closing secondary fractures would be displaced into the surrounding matrix during the later stage of production, irrespective to the  $K_{rw}$  functions. This may explain why there are almost no observable differences in the water production profiles as  $K_{rw}$  varies (Figure 28a). In Figure 28 (b), different water volumes in the near-well matrix are observed for the three cases during the soaking period; however, as soon as the production period commences and the secondary fractures start to close, the water volumes are the same among the three cases.

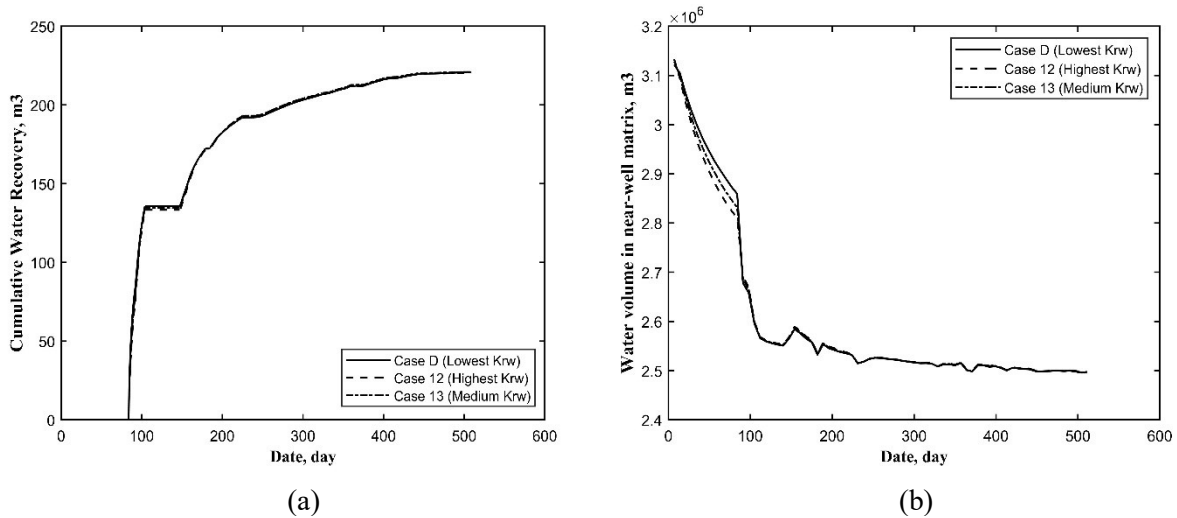


Figure 28. (a) Cumulative water recovery and (b) water volume in the near-well matrix corresponding to various matrix water relative permeability functions.

### 5.3.3 Effects of Matrix Gas Relative Permeability

To examine the sensitivity of matrix gas relative permeability on recovery performance, Cases 14 and 15 with the following gas relative permeability functions (the same as section 4.4.5) are examined:  $K_{rg \text{ Case D}} > K_{rg \text{ Case 14}} > K_{rg \text{ Case 15}}$ . Secondary fracture closure is considered in all three cases. The corresponding gas production profiles are compared with the Case D in Figure 29 (a).

As  $K_{rg}$  increases, gas production would increase; and a further exaggerated increase in gas production for a higher  $K_{rg}$  is observed, as compared to the gas production files in section 4.4.5 where fracture closure is not considered (Figure 19a). This is because the benefit of a higher gas mobility is further emphasized when fracture closure is considered; as the near-well secondary fractures are closed, it becomes easier for the gas to be produced if  $K_{rg}$  in the matrix is further increased. As shown in Figure 29 (b), less gas remains in the near-well matrix if  $K_{rg}$  is increased.

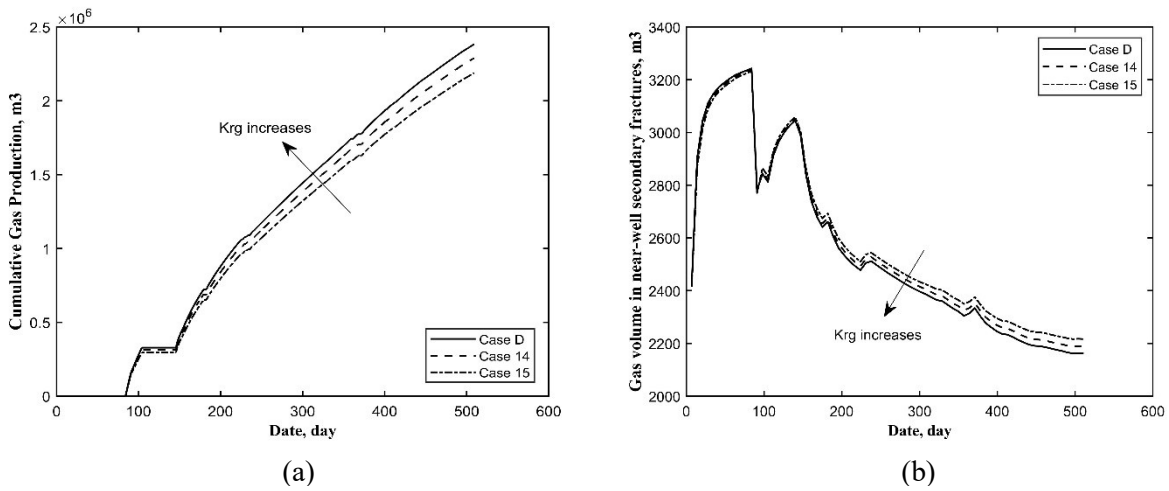


Figure 29. (a) Cumulative gas production and (b) gas volume in near-well matrix corresponding to different matrix gas relative permeability functions.

### 5.3.4 Effects of Shut-in Duration

Shut-in duration is often an important operating decision that is to be optimized. To examine the impacts of shorter shut-in durations on the recovery performance, two additional cases, Cases 16 (with 8 weeks of shut-in) and Case 17 (with 2 weeks of shut-in), are studied. The corresponding gas productions profiles are compared with Case D (with 12 weeks of shut-in) in Figure 30 (a). A prolonged shut-in duration is likely to induce a similar impact on gas production as that of a higher matrix  $P_c$ , with both resulting in more gas being displaced to the secondary fractures and more water being imbibed into the matrix (less water recovery). Therefore, similar to the results

presented in Figure 27, Case D (with 12 weeks of shut-in) also yields the lowest gas production (particularly at the early times), with the highest gas volume residing in the secondary fractures and highest water volume in the near-well matrix, as shown in Figure 30 (a), (b) and (c). This observation would suggest that a shorter shut-in duration is preferred for shale gas reservoirs. This conclusion is contrary to several previous studies where secondary fracture closure was ignored (e.g., Wang and Leung, 2015a, b); it was reported in those studies that although shorter shut-in may be beneficial to water recovery, little to no improvement in long-term hydrocarbons production was observed.

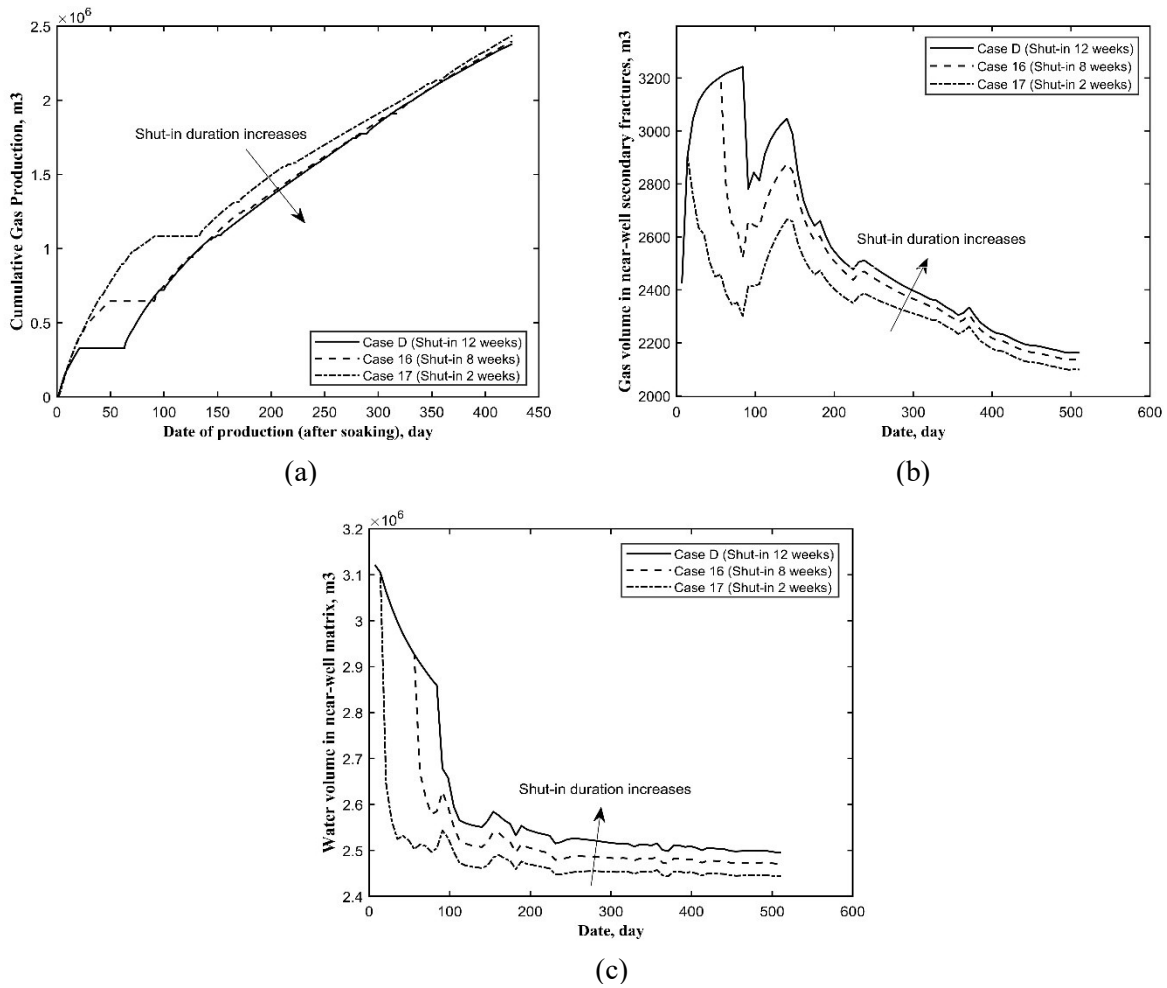


Figure 30. (a) Cumulative gas production; (b) gas volume in near-well secondary fractures; and (c) water volume in the near-well matrix corresponding to various shut-in durations (12, 8 and 2 weeks).

## **Chapter 6: Conclusions and Future Work**

In this study, by incorporating the apparent permeability modeling, secondary fracture network modeling and secondary fracture closure modeling in the numerical simulation, several potential scenarios of water loss, along with the associated implications on fracturing design, optimal operational strategies and estimation of stimulated reservoir volume are investigated. Conclusions from this study and recommendations for future study are provided in this chapter.

### **6.1 Conclusions**

1. This work presents a set of detailed simulation studies, where modeling of realistic configurations of stochastic 3D discrete fracture network, apparent permeability and fracture closure are coupled. A novel, yet practical, pressure-dependent matrix apparent permeability modeling scheme is implemented to incorporate the non-Darcy flow behavior due to the transport mechanisms taken place in the nanopores. A novel method involving rock-type indicators is introduced to represent the open and closed states of secondary fracture, facilitating the modeling of stress-dependent closure of the secondary fracture system. Most importantly, the entire coupling workflow can be readily implemented in most commercial reservoir simulation packages.

2. The developed models are used to examine production behavior and fracturing fluid distribution during soaking and flow-back periods as well as the various scenarios that may be responsible for water blockage, particularly in the presence of disconnected secondary fractures.

3. For a certain observed gas production, neglecting the effects of secondary fractures and apparent permeability ( $K_{app}$ ) modeling would overestimate the contribution of hydraulic fracture on gas production. It is generally observed that improved overall conductivity due to the secondary fractures and enhanced matrix permeability would increase both gas production and water loss.

4. Fluid distribution in the region near the hydraulic fracture is most sensitive to a number of factors including secondary fracture connectivity,  $K_{app}$  modeling, as well as matrix multiphase flow functions; however, the extent to which the fracturing fluid could imbibe into the matrix is mainly affected by the secondary fracture connectivity.

5. Sensitivity analysis of the matrix multiphase flow functions is performed. If the secondary fracture closure is neglected, it is concluded that, except for an increase in the matrix gas relative permeability, gas and water productions are typically inversely related to the amount of water in the near-well region; several different trends are observed in this study of shale gas production, in comparison to previous findings involving a water-oil system: an increase in compressibility for the gas-oil systems has rendered the gas flow from matrix due to countercurrent imbibition to be less prominent.

6. Neglecting the effects of fracture closure and the resulting water blockage could potentially overestimate the contribution of secondary fracture network for a certain observed gas production.

7. Secondary fractures may close during flowback and production; secondary fracture closure

would displace the fluids residing in the closing secondary fractures into the surrounding matrix as the production period continues. A larger volume of gas could be retained in the fractures, while a larger amount of water may accumulate in the near-well region – this may potentially contribute to some degree of water blockage in the near-well region, hindering the gas flow to the well; however, a reduction in water loss is also observed due to an increase in water saturation and pressure in the near-well matrix.

8. If secondary fracture closure is considered, the sensitivity analysis would indicate that water recovery is less sensitive to variations in the relative mobility of the water phase, as water displaced from the closing secondary fractures would imbibe into the surrounding matrix eventually; gas and water production is enhanced whenever matrix imbibition is reduced; this is particularly important in the case of shut-in duration: shorter shut-in periods would be beneficial to gas production and water recovery. This conclusion is contrary to several previous studies when secondary fracture closure was ignored; those studies reported little to no improvement in long-term production, despite a spike in initial production was observed.

## **6.2 Future Work**

1. In our study, it is assumed that secondary fractures would close abruptly and also completely once the fracture pressure drops below the fracture closure stress. However, according to Wang and Sharma (2018), “fracture closure is a gradual process”; and Batzle et al. (1980) indicated that “Natural cracks have walls that are irregular, etched and pitted, and poorly matched. Closure is incomplete with many portions of the crack remaining open and interconnected”. Therefore, in the

future work, a progressive fracture closure model involving multiple stages of closure could be implemented; in addition, the behavior of incomplete fracture closure due to the presence of surface asperities or proppant distribution should be further investigated.

2. Although our work primarily focuses on the water-gas system, the modeling could also be extended to water-oil system, such as simulating the tight oil reservoirs, to examine if the conclusions obtained from our study (e.g. shorter shut-in duration is beneficial for gas production) are still applicable for those oil reservoirs.

3. In our study, it is assumed that the main hydraulic fracture is a regular cuboid, its two wings are symmetrical about the production well, and every cell of HF is assigned with identical properties (e.g., permeability, porosity and pressure). However, in reality, the hydraulic fracture size, permeability and other properties often vary along the fracture length, which could potentially influence the fluid distribution around the well. Therefore, in the future work, incorporating a more realistic main hydraulic fracture which could be generated by some reliable hydraulic-fracture-propagation models in the reservoir simulation could be considered.

4. Shale gas reservoirs often have thermodynamic properties that are different from the conventional reservoirs. Neglecting the effects of thermodynamic properties might result in inaccurate estimations for fracturing fluid loss or overall stimulated reservoir volume. Therefore, in the future work, incorporating the thermodynamic effect that is corresponding to a certain shale gas reservoir in the reservoir simulation could be considered for improving the estimation

accuracy.

## Bibliography

- Agrawal, S., & Sharma, M. M. (2015). Practical insights into liquid loading within hydraulic fractures and potential unconventional gas reservoir optimization strategies. *Journal of Unconventional Oil and Gas Resources*, 11, 60-74.
- Aguilar-Armenta, G., Hernandez-Ramirez, G., Flores-Loyola, E., Ugarte-Castaneda, A., Silva-Gonzalez, R., Tabares-Munoz, C., Jimenez-Lopez, A., & Rodriguez-Castellon, E. (2001). Adsorption kinetics of CO<sub>2</sub>, O<sub>2</sub>, N<sub>2</sub>, and CH<sub>4</sub> in cation-exchanged clinoptilolite. *The Journal of Physical Chemistry B*, 105(7), 1313-1319.
- Alkouh, A., McKetta, S., & Wattenbarger, R. A. (2014). Estimation of effective-fracture volume using water-flowback and production data for shale-gas wells. *Journal of Canadian Petroleum Technology*, 53(05), 290-303.
- Anderson, D. M., Turco, F., Virues, C. J. J., & Chin, A. (2013). Application of rate transient analysis workflow in unconventional reservoirs: Horn river shale gas case study. Paper SPE-167042-MS presented at the SPE Unconventional Resources Conference and Exhibition-Asia Pacific, Brisbane, Australia, Nov. 11-13.
- Arkilic, E. B., Breuer, K. S., & Schmidt, M. A. (2001). Mass flow and tangential momentum accommodation in silicon micromachined channels. *Journal of Fluid Mechanics*, 437, 29-43.
- Aziz, K. (1979). *Petroleum reservoir simulation*. Applied Science Publishers, 476 pp., Applied Science Publishers, London, United Kingdom.
- Azom, P. N., & Javadpour, F. (2012). Dual-continuum modeling of shale and tight gas reservoirs. Paper SPE-159584-MS presented at SPE Annual Technical Conference and Exhibition, San Antonio, Texas, USA, Oct. 8-10.
- Barenblatt, G. I., Zheltov, I. P., & Kochina, I. N. (1960). Basic concepts in the theory of seepage of homogeneous liquids in fissured rocks [strata]. *Journal of Applied Mathematics and Mechanics*, 24(5), 1286-1303.
- Barfield, E. C., Jordan, J. K., & Moore, W. D. (1959). An analysis of large-scale flooding in the fractured Spraberry trend area reservoir. *Journal of Petroleum Technology*, 11(04), 15-19.

- Batzle, M. L., Simmons, G., & Siegfried, R. W. (1980). Microcrack closure in rocks under stress: Direct observation. *Journal of Geophysical Research: Solid Earth*, 85(B12), 7072-7090.
- Beaudoin, B., Allison, J., Khalid, S., & Faurichou, K. (2011). Horn River Basin: A Study of the Behavior of Frac Barriers in a Thick Shale Package Using the Integration of Microseismic, Geomechanics and Log Analysis, Paper SPE-147510-MS presented at the Canadian Unconventional Resources Conference held in Calgary, Alberta, Canada, Nov. 15-17.
- Belyadi, H., Fathi, E., & Belyadi, F. (2019). Hydraulic fracturing in unconventional reservoirs: theories, operations, and economic analysis. Gulf Professional Publishing.
- Bradley, H. B. (1987). *Petroleum engineering handbook*, third edition SPE, Richardson, Texas (Chapter 26).
- Chalmers, G.R., Ross, D.J. and Bustin, R.M. (2012). Geological controls on matrix permeability of Devonian Gas Shales in the Horn River and Liard basins, northeastern British Columbia, Canada. *International Journal of Coal Geology*, 103: 120-131.
- Cheng, Y. (2012), Impact of water dynamics in fractures on the performance of hydraulically fractured wells in gas-shale reservoirs, *J. Can. Pet. Technol.*, 51(2), 143–151.
- Cho, Y., Ozkan, E., & Apaydin, O. G. (2013). Pressure-dependent natural-fracture permeability in shale and its effect on shale-gas well production. *SPE Reservoir Evaluation & Engineering*, 16(02), 216-228.
- Cipolla, C. L. (2009). Modeling production and evaluating fracture performance in unconventional gas reservoirs. *Journal of Petroleum Technology*, 61(09), 84-90.
- Civan, F. (2010). Effective correlation of apparent gas permeability in tight porous media. *Transport in Porous Media*, 82(2), 375-384.
- Civan, F., Rai, C. S., & Sondergeld, C. H. (2011). Shale-gas permeability and diffusivity inferred by improved formulation of relevant retention and transport mechanisms. *Transport in porous media*, 86(3), 925-944.
- Coppens, M. (1999). The effect of fractal surface roughness on diffusion and reaction in porous catalysts—from fundamentals to practical applications. *Catalysis Today*, 53(2), 225-243.

- Coppens, M., & Dammers, A. J. (2006). Effects of heterogeneity on diffusion in nanopores—from inorganic materials to protein crystals and ion channels. *Fluid Phase Equilibria*, 241(1-2), 308-316.
- Darabi, H., Eftehad, A., Javadpour, F., & Sepehrnoori, K. (2012). Gas flow in ultra-tight shale strata. *Journal of Fluid Mechanics*, 710, 641-658.
- Dershowitz, B., LaPointe, P., Eiben, T., & Wei, L. (1998). Integration of discrete feature network methods with conventional simulator approaches. Paper SPE-49069-MS presented at the SPE Annual Technical Conference and Exhibition, New Orleans, Louisiana, USA, Sep. 27-30.
- Dershowitz, W. S., Cottrell, M. G., Lim, D. H., & Doe, T. W. (2010). A discrete fracture network approach for evaluation of hydraulic fracture stimulation of naturally fractured reservoirs. Paper presented at the 44th US Rock Mechanics Symposium and 5th US-Canada Rock Mechanics Symposium, Salt Lake City, Utah, USA, Jun. 27-30.
- Dong, J., Hsu, J., Wu, W., Shimamoto, T., Hung, J., Yeh, E., Wu, Y., & Sone, H. (2010). Stress-dependence of the permeability and porosity of sandstone and shale from TCDP hole-A. *International Journal of Rock Mechanics and Mining Sciences*, 47(7), 1141-1157.
- Economides, M. J., & Nolte, K. G. (1989). *Reservoir stimulation* (Vol. 2). Englewood Cliffs, NJ: Prentice Hall.
- Evans, R. D., & Civan, F. (1994). Characterization of non-Darcy multiphase flow in petroleum bearing formation. Final report (No. DOE/BC/14659-7). Oklahoma Univ., Norman, OK (United States). School of Petroleum and Geological Engineering.
- Fakcharoenphol, P., Torcuk, M. A., Wallace, J., Bertoncello, A., Kazemi, H., Wu, Y., & Honarpour, M. (2013). Managing shut-in time to enhance gas flow rate in hydraulic fractured shale reservoirs: A simulation study. Paper SPE-166098-MS presented at the SPE Annual Technical Conference and Exhibition, New Orleans, Louisiana, USA, Sep. 30 – Oct. 2.
- Farah, N. (2016). *Flow modelling in low permeability unconventional reservoirs* (Doctoral dissertation, Paris 6).
- Gale, J. F., Laubach, S. E., Olson, J. E., Eichhubl, P., & Fall, A. (2014). Natural fractures in shale: A review and new observations. *AAPG Bulletin*, 98(11), 2165-2216.

- Gangi, A. F. (1978). Variation of whole and fractured porous rock permeability with confining pressure. Paper presented at the International Journal of Rock Mechanics and Mining Sciences & Geomechanics Abstracts, 15(5) 249-257.
- Gdanski, R.D., Fulton, D.D., & Shen, C., (2009). Fracture–face–skin evolution during cleanup. J. SPE Prod. Oper. 24, 22–34.
- Gensterblum, Y., Ghanizadeh, A., Cuss, R.J et al. (2015). Gas transport and storage capacity in shale gas reservoirs—A review. Part A: transport processes. Journal of Unconventional Oil and Gas Resources, 12: 87-122.
- Ghanbari, E., & Dehghanpour, H. (2016). The fate of fracturing water: A field and simulation study. Fuel, 163, 282-294.
- Guo, C., Xu, J., Wu, K., Wei, M., & Liu, S. (2015). Study on gas flow through nano pores of shale gas reservoirs. Fuel, 143, 107-117.
- Holditch, S. A. (1979). Factors affecting water blocking and gas flow from hydraulically fractured gas wells. Journal of Petroleum Technology, 31(12), 1,524.
- Hunter, C. D., & Young, D. M. (1953). Relationship of natural gas occurrence and production in eastern Kentucky (big sandy gas field) to joints and fractures in Devonian bituminous shale. AAPG Bulletin, 37(2), 282-299.
- Huo, D., Li, B., & Benson, S.M. (2014). Investigating Aperture-based Stress-dependent Permeability and Capillary Pressure in Rock Fractures. Paper SPE-170879-MS, presented at the SPE Annual Technical Conference and Exhibition, held in Amsterdam, The Netherlands, Oct. 27-29.
- H. Singh, F. Javadpour, A. Etehadavakkol, & H. Darabi. (2014). Nonempirical apparent permeability of shale. SPE Reservoir Eval. Eng. 17 (03) (2014) 414–424.
- Jang, H., & Lee, J. (2015). Effect of fracture design parameters on the well performance in a hydraulically fractured shale gas reservoir. Energy Exploration & Exploitation, 33(2), 157-168.
- Javadpour, F. (2009). Nanopores and apparent permeability of gas flow in mudrocks (shales and siltstone). Journal of Canadian Petroleum Technology, 48(08), 16-21.

- Javadpour, F., Fisher, D. & Unsworth, M. (2007). Nanoscale gas flow in shale sediments. *J. Can. Petrol. Technol.* 46 (10), 55–61.
- Karimi-Fard, M., Durlofsky, L. J., & Aziz, K. (2003). An efficient discrete fracture model applicable for general purpose reservoir simulators. Paper SPE-79699-MS presented at the SPE Reservoir Simulation Symposium, Houston, Texas, USA, Feb. 3-5.
- Khlaifat, A.L., Qutob, H., & Barakat, N. (2011). Tight gas sands development is critical to future world energy resources. Paper SPE-142049-MS, presented at SPE Middle East Unconventional Gas Conference and Exhibition, Muscat, Oman, Jan. 31-Feb. 2.
- King, G. E. (2010). Thirty years of gas shale fracturing: What have we learned? Paper SPE-133456-MS presented at the SPE Annual Technical Conference and Exhibition, Florence, Italy, Sep. 19-22.
- Knudsen, M. (1909). Die gesetze der molekularströmung und der inneren reibungsströmung der gase durch röhren. *Annalen Der Physik*, 333(1), 75-130.
- Le, M. T. (2018). An assessment of the potential for the development of the shale gas industry in countries outside of North America. *Heliyon*, 4(2), e00516.
- Leverett, M. (1941). Capillary behavior in porous solids. *Transactions of the AIME*, 142(01), 152-169.
- Liu, Y., Leung, J.Y., & Chalaturnyk, R. (2018). Geomechanical simulation of partially-propped fracture closure and its implication on water flowback and gas production. *SPE Reservoir Evaluation & Engineering* SPE Reservoir Evaluation & Engineering 21(2): 273-290 (selected to appear as a spotlight paper on Unconventional Resources).
- Liu, Y., Leung, J. Y. W., Chalaturnyk, R. J., & Virués, C. J. J. (2019). New insights on mechanisms controlling fracturing-fluid distribution and their effects on well performance in shale-gas reservoirs. *SPE Production & Operations*.
- Makhanov, K., Habibi, A., Dehghanpour, H., & Kuru, E. (2014). Liquid uptake of gas shales: A workflow to estimate water loss during shut-in periods after fracturing operations. *Journal of Unconventional Oil and Gas Resources*, 7, 22-32.
- MATLAB. (2019). Version 9.6 (R2019a). Natick, Massachusetts: The MathWorks Inc.

- Mayerhofer, M. J., & Meehan, D. N. (1998). Waterfracs-Results from 50 cotton valley wells. Paper SPE-49104-MS presented at the SPE Annual Technical Conference and Exhibition, New Orleans, LA, USA, Sep. 27-30.
- McClure, MW. (2014). The potential effect of network complexity on recovery of injected fluid following hydraulic fracturing. Paper SPE-168991-MS presented in the SPE unconventional resources conference, held in The Woodlands, TX, USA, April 1–3.
- McClure, M. W., & Horne, R. N. (2014). An investigation of stimulation mechanisms in enhanced geothermal systems. *International Journal of Rock Mechanics and Mining Sciences*, 72, 242-260.
- McClure, M. W., & Zoback, M. D. (2013). Computational investigation of trends in initial shut-in pressure during multi-stage hydraulic stimulation in the Barnett shale. Paper presented at the 47th US Rock Mechanics/Geomechanics Symposium, held in San Francisco, CA, USA, June 23-26.
- Mckernan, R.E., Rutter, E.H., Mecklenburgh, J., Taylor, K.G., & Covey-Crump, S.J. (2014). Influence of effective pressure on mudstone matrix permeability: implications for shale gas production. Paper SPE-167762-MS presented at the SPE/EAGE European Unconventional Conference and Exhibition, held in Vienna, Austria, Feb. 25–27.
- Meyer, B. R., & Bazan, L. W. (2011). A Discrete Fracture Network Model for Hydraulically Induced Fractures - Theory, Parametric and Case Studies. Society of Petroleum Engineers. doi:10.2118/140514-MS.
- Mi, L., Jiang, H., Cao, Y., Fang, S., Liu, H., Zhou, Y., An, C., & Yan, B. (2019). Comprehensive apparent permeability model coupled shale gas transfer mechanisms in natural fractures and matrix. *Journal of Petroleum Science and Engineering*, 172, 878-888.
- Nejadi, S., Leung, J. Y., Trivedi, J. J., & Virués, C. (2015). Integrated characterization of hydraulically fractured shale-gas Reservoirs—Production history matching. *SPE Reservoir Evaluation & Engineering*, 18(04), 481-494.
- Ning, X., Fan, J. & Lancaster D.E. (1993). Measurement of Shale Matrix and Fracture Properties in Naturally Fractured Cores Using Pulse Testing. *Gas Shales Technology Review* (October 1993) 8, 2, 31-45.

- Novlesky, A., Kumar, A., & Merkle, S. (2011). Shale Gas modeling workflow: from microseismic to simulation -- a Horn River case study. Paper SPE-148710-MS presented at Canadian Unconventional Resources Conference, Calgary, Alberta, Canada, Nov. 15-17.
- Oda, M. (1985). Permeability tensor for discontinuous rock masses. *Geotechnique*, 35(4), 483-495.
- Oil, B. C., & Gas Commission. (2014). Horn River Basin unconventional shale gas play atlas. BC Oil & Gas Commission Publications.
- Prausnitz, J. M., & Benson, P. R. (1959). Solubility of liquids in compressed hydrogen, nitrogen, and carbon dioxide. *AIChE Journal*, 5(2), 161-164.
- Qasem, F. H., Nashawi, I. S., Gharbi, R., & Mir, M. I. (2008). Recovery performance of partially fractured reservoirs by capillary imbibition. *Journal of Petroleum Science and Engineering*, 60(1), 39-50.
- Reinicke, A., Rybacki, E., Stanchits, S., Huenges, E., & Dresen, G. (2010). Hydraulic fracturing stimulation techniques and formation damage mechanisms—Implications from laboratory testing of tight sandstone–proppant systems. *Chemie Der Erde-Geochemistry*, 70, 107-117.
- Rogers, S., Elmo, D., Dunphy, R., & Bearinger, D. (2010). Understanding hydraulic fracture geometry and interactions in the Horn River basin through DFN and numerical modeling. Paper SPE-137488-MS presented at the Canadian Unconventional Resources and International Petroleum Conference, Calgary, Alberta, Canada, Oct. 19-21.
- Roy, S., Raju, R., Chuang, H. F., Cruden, B. A., & Meyyappan, M. (2003). Modeling gas flow through microchannels and nanopores. *Journal of Applied Physics*, 93(8), 4870-4879.
- Rubin, B. (2010). Accurate simulation of non-Darcy flow in stimulated fractured shale reservoirs. Paper SPE-132093-MS presented at the SPE Western Regional Meeting, Anaheim, California, USA, May. 27-29.
- Rubin, C., Zamirian, M., Takbiri-Borujeni, A., & Gu, M. (2019). Investigation of gas slippage effect and matrix compaction effect on shale gas production evaluation and hydraulic fracturing design based on experiment and reservoir simulation. *Fuel*, 241, 12-24.

- Sabathier, J. C., Bourbiaux, B. J., Cacas, M. C., & Sarda, S. (1998). A new approach of fractured reservoirs. Paper SPE-39825-MS presented at the International Petroleum Conference and Exhibition of Mexico, Villahermosa, Mexico, Mar. 3-5.
- Sakhaee-Pour, A., & Bryant, S. (2012). Gas permeability of shale. *SPE Reservoir Evaluation & Engineering*, 15(04), 401-409.
- Schrauf, T. W., & Evans, D. D. (1986). Laboratory studies of gas flow through a single natural fracture. *Water Resources Research*, 22(7), 1038-1050.
- Shanley, K. W., Cluff, R. M., & Robinson, J. W. (2004). Factors controlling prolific gas production from low-permeability sandstone reservoirs: Implications for resource assessment, prospect development, and risk analysis. *AAPG Bulletin*, 88(8), 1083-1121.
- Shaoul, J. R., van Zelm, L. F., & De Pater, C. J. (2011). Damage mechanisms in unconventional-gas-well stimulation--a new look at an old problem. *SPE Production & Operations*, 26(04), 388-400.
- Sherman, J. B., & Holditch, S. A. (1991). Effect of injected fracture fluids and operating procedures on ultimate gas recovery. Paper SPE-21496-MS presented at the SPE Gas Technology Symposium, Houston, TX, USA, Jan. 23-25.
- Shi, J., Zhang, L., Li, Y., Yu, W., He, X., Liu, N., Li, X., & Wang, T. (2013). Diffusion and flow mechanisms of shale gas through matrix pores and gas production forecasting. Paper SPE-167226-MS presented at the SPE Unconventional Resources Conference Canada, Calgary, Alberta, Canada, Nov. 5-7.
- Shiozawa, S., & McClure, M. (2016). Simulation of proppant transport with gravitational settling and fracture closure in a three-dimensional hydraulic fracturing simulator. *Journal of Petroleum Science and Engineering*, 138, 298-314.
- Song, W., Yao, J., Li, Y., Sun, H., Zhang, L., Yang, Y., Zhao, J., & Sui, H. (2016). Apparent gas permeability in an organic-rich shale reservoir. *Fuel*, 181, 973-984.
- Vesovic Velisa. (2011). METHANE. Website, 2011. <http://www.thermopedia.com/content/951/>  
doi: 10.1615/AtoZ.m.methane.

- Walsh, J. B. (1965). The effect of cracks on the uniaxial elastic compression of rocks. *Journal of Geophysical Research*, 70(2), 399-411.
- Wang, C., Wu, Y.S., Xiong, Y., Winterfeld, P.H., & Huang, Z. (2015). Geomechanics Coupling Simulation of Fracture Closure and Its Influence on Gas Production in Shale Gas Reservoirs. Paper SPE-173222-MS presented at SPE Reservoir Simulation Symposium, Houston, Texas, Feb. 23–25.
- Wang, H., & Sharma, M. M. (2018). Estimating Fracture Closure Stress in Naturally Fractured Reservoirs with Diagnostic Fracture Injection Tests. Paper 2018-225 ARMA presented at the 52<sup>nd</sup> U.S. Rock Mechanics/Geomechanics Symposium Conference, Seattle, Washington, Jun. 17–20.
- Wang, M., & Leung, J. Y. (2015a). Numerical investigation of coupling multiphase flow and geomechanical effects on water loss during hydraulic fracturing flow back operation. Paper presented at the Unconventional Resources Technology Conference, San Antonio, Texas, Jul. 20-22.
- Wang, M., & Leung, J. Y. (2015b). Numerical investigation of fluid-loss mechanisms during hydraulic fracturing flow-back operations in tight reservoirs. *Journal of Petroleum Science and Engineering*, 133, 85-102.
- Wang, M., & Li, Z. (2004). Micro-and nanoscale non-ideal gas poiseuille flows in a consistent Boltzmann algorithm model. *Journal of Micromechanics and Microengineering*, 14(7), 1057.
- Warren, J. E., & Root, P. J. (1963). The behavior of naturally fractured reservoirs. *Society of Petroleum Engineers Journal*, 3(03), 245-255.
- Wattenbarger, R. A., & Alkough, A. B. (2013). New advances in shale reservoir analysis using flowback data. Paper SPE-165721-MS presented at the SPE Eastern Regional Meeting, Pittsburgh, Pennsylvania, USA, Aug. 20-22.
- Wilkinson, W. M. (1953). Fracturing in Spraberry reservoir, west Texas. *AAPG Bulletin*, 37(2), 250-265.
- Wu, K., & Olson, J. E. (2016). Numerical investigation of complex hydraulic-fracture development in naturally fractured reservoirs. *SPE Production & Operations*, 31(04), 300-309.

- Wu, K., Chen, Z., & Li, X. (2015). Real gas transport through nanopores of varying cross-section type and shape in shale gas reservoirs. *Chemical Engineering Journal*, 281, 813-825.
- Wu, K., Li, X., Wang, C., Chen, Z., & Yu, W. (2015). A model for gas transport in microfractures of shale and tight gas reservoirs. *AIChE Journal*, 61(6), 2079-2088.
- Xu, Y., Adefidipe, O., & Dehghanpour, H. (2016). A flowing material balance equation for two-phase flowback analysis. *Journal of Petroleum Science and Engineering*, 142, 170-185.
- Yang, S., Harris, N. B., Dong, T., Wu, W., & Chen, Z. (2018). Natural fractures and mechanical properties in a Horn River shale core from well logs and hardness measurements. *SPE Reservoir Evaluation & Engineering*, 21(03), 671-682.
- Yousefzadeh, A., Li, Q., Virues, C., & Aguilera, R. (2016). Integrated interpretation of microseismic and petroleum engineering data for comparison of gas production in two interfering adjacent wellpads in the Horn River basin, Canada. Paper presented at the Unconventional Resources Technology Conference, San Antonio, Texas, Aug. 1-3.
- Yu, W., & Sepehrnoori, K. (2014a). Simulation of gas desorption and geomechanics effects for unconventional gas reservoirs. *Fuel*, 116, 455-464.
- Yu, W., & Sepehrnoori, K. (2014b). Optimization of Well Spacing for Bakken Tight Oil Reservoirs. Paper URTEC-1922108-MS presented at the Unconventional Resources Technology Conference, Denver, Colorado, USA, Aug. 25-27. doi:10.15530/URTEC-2014-1922108.
- Yu, W., Zhang, T., Du, S., & Sepehrnoori, K. (2015). Numerical study of the effect of uneven proppant distribution between multiple fractures on shale gas well performance. *Fuel*, 142, 189-198.
- Zhang, L., Shan, B., Zhao, Y., Du, J., Chen, J., & Tao, X. (2018). Gas transport model in organic shale nanopores considering Langmuir slip conditions and diffusion. Pore confinement, real gas, and geomechanical effects. *Energies*, 11(1), 223.
- Zhong, Y., Zhang, H., Shao, Z., & Li, K. (2015). Gas transport mechanisms in micro-and nano-scale matrix pores in shale gas reservoirs. *Chemistry and Technology of Fuels and Oils*, 51(5), 545-555.